Development of Dense Ceramic Tiles from Mixtures of Alumina Powders with Different PSD

By

Mücahit SÜTÇÜ

**A Dissertation Submitted to the
Graduate School in Partial Fulfillment of the
Requirements for the Degree of**

MASTER OF SCIENCE

**Programme: Materials Science and Engineering
Major: Materials Science and Engineering**

**İzmir Institute of Technology
İzmir, Turkey**

July, 2004

We approve the thesis of **Mücahit Sütçü**

Date of Signature

---------- **30.07.2004**

Assoc. Prof. Dr. Sedat AKKURT
Supervisor

Department of Mechanical Engineering

---------- **30.07.2004**

Prof. Dr. Muhsin ÇİFTÇİOĞLU

Co-Supervisor

Department of Chemical Engineering

---------- **30.07.2004**

Assoc. Prof. Dr. Metin TANOĞLU
Co-Supervisor

Department of Mechanical Engineering

---------- **30.07.2004**

Assoc. Prof. Dr. Funda TIHMINLIOĞLU

Department of Chemical Engineering

---------- **30.07.2004**

Asst. Prof. Dr. Fehime ÖZKAN

Department of Chemical Engineering

---------- **30.07.2004**

Prof. Dr. Muhsin ÇİFTÇİOĞLU

Head of Materials Science and Engineering Programme

ACKNOWLEDGMENTS

I would like to thank my advisor Assoc. Prof. Dr. Sedat Akkurt for his guidance and encouragement. He shared his all knowledge and expertise with me during this research. I am also very thankful to Assoc. Prof. Dr. Ahmet Eroğlu, IZTECH CMR and IZTECH Atelier staff because of their helps during the experimental and production steps of the study. Finally, I would like to thank my family for their patience and support.

ABSTRACT

In Turkey, domestic alumina powders are generally used as an intermediate product in metallic aluminum production. Recently, its usage as a raw material for technical applications in ceramic industry has gained importance.

The properties of domestic powders must be improved in order to be used in technical ceramic applications. Because these powders have coarse particle size with a high amount of sodium oxide as well as incomplete transformation to stable form. Therefore, sodium oxide that has been physically and chemically bound to aluminum oxide during Bayer process must be removed. In this study, sodium oxide (Na_2O) content of the domestic powders was decreased to desirable levels (<0.15% Na_2O) by hot washing treatments. These powders were calcined to transform into stable alpha form. X-Ray Diffraction (XRD) was preformed to analyze the calcined and as-received powders. Chemical analyses of the powders were done using Atomic Absorption Spectrometry (AAS) and Inductively Coupled Plasma-Atomic Emission Spectrometry (ICP-AES). Domestic powders were ground. Scanning Electron Microscopy (SEM) was performed to analyze the morphology and particle size distributions of as-received and ground powders. Particle size distributions (PSD) were plotted using lineal intercept method.

In this study, it was aimed to provide maximum packing by blending the powders in different combinations (binary and ternary powder blends). In addition to this, dense ceramic tiles were produced by blending different proportions of the powders that provide maximum packing. In this study, the improved domestic (coarse size-SKA and medium size-SEA) and superground (Alcoa CT3000SG) alumina powders with three different particle size distributions were used. The packing of binary (SEA-CT3000SG) and ternary (SKA-SEA-CT3000SG) blends were predicted by using the softwares, MXENTRY® and MIX10®. These softwares utilized the Dinger-Funk (DF) equation for predictions of packing. Prepared blends were uniaxially dry-pressed and sintered. Archimedes' method was used to measure the density and porosity of the pellets. All results showed that the blend contained 100% superground alumina powders achieved almost full density (98%) at 1550°C. The binary and ternary blends that contained a relatively higher proportion of fine alumina powders provided higher fired

densities. In binary blends, if the proportion of SEA was up to 50%, porosity values of these blends increased.

Also the effects of additives such as TiO_2 and MnO_2 on densification and mechanical properties of pellets were investigated. The additives provided higher fired densities between 91 and 99%.

Vickers hardness tests were conducted to determine mechanical properties of the sintered pellets. The samples that contained relatively higher proportions of fine particles provided higher hardness values in a range of 1500 and 2100 $kg.mm^{-2}$. Also, microstructural characterization of the pellets was done using SEM.

Finally, the tiles at desired dimensions were produced based on the blends that give the highest density and hardness values. Porosity and density measurements, microstructural and mechanical characterizations of the tiles were carried out.

ÖZ

Ülkemizde genellikle metalik aluminyum üretiminde ara ürün olarak kullanılan yerli üretim aluminanın seramik endüstrisinde teknik seramik hammaddesi olarak kullanılması son zamanlarda önem kazanmıştır. Bu durum gözönüne alınarak tez çalışmasında yerel tozlarla birlikte ithal tozların farklı kombinasyonlarda karıştırılması sonucu yoğun seramik fayansların elde edilebileceği düşünülmüştür.

Yerel alumina tozun teknik seramik olarak kullanılabilmesi için özelliklerinin iyileştirilmesi gerekmektedir. Yerel tozlar iri tanelidir ve yüksek miktarda sodyum oksit (Na_2O) içerir, ayrıca tam olarak kararlı yapıya dönüşmemiştir. Bunun için tozların bünyesindeki üretim esnasında fiziksel ve kimyasal olarak bağlanmış olan sodanın yapıdan uzaklaştırılması gerekmektedir. Bu çalışmada sıcak yıkama işlemiyle tozların sodyum oksit içeriği uygun seviyelere (<%0.15 Na_2O) düşürülmüştür. Yerel tozların kararlı alfa fazına dönüştürülmesi için kalsine edilmişlerdir. Orjinal ve kalsine edilmiş tozların faz karakterizasyonu X-Işını Kırınımı (XRD) cihazı ile yapılmıştır. Tozların kimyasal analizleri için Atomik Absopsiyon Spektrometre (AAS) ve Endüktif Eşleşmiş Plazma-Atomik Emisyon Spektrometre (ICP-AES) cihazları kullanılmıştır. İri taneli bu tozlar öğütme işlemine tabi tutulmuşlardır. Orjinal ve öğütülen tozların morfolojisi ve tane boyutu analizi için Taramalı Elektron Mikroskobu (SEM) resimleri kullanılmıştır. Tozların tane boyut dağılımları çizgisel kesişme metodu kullanılarak çizilmiştir.

Bu çalışmada, farklı tane boyut dağılımına sahip yerel Bayer ve süper öğütülmüş alumina tozların farklı kombinasyonlarda (ikili ve üçlü toz karışımları) karıştırılıp maximum paketlenebilirliğinin sağlanmasına çalışılmıştır. Böylelikle maximum yoğunlaşmanın sağlandığı karışımlardan yoğun seramik fayanslar üretilmiştir. Bu çalışmada özellikleri iyileştirilmiş yerel Bayer (iri boyutlu-SKA ve orta boyutlu-SEA) ve süper öğütülmüş (Alcoa CT3000SG) tozlar olmak üzere üç farklı tane boyut dağılımına sahip alumina toz kullanılmıştır. İkili (SEA-CT3000SG) ve üçlü (SKA-SEA-CT3000SG) toz karışımlarının paketlenmesi MXENTRY ve MIX10 gibi bilgisayar yazılımları kullanılarak sağlanmıştır. Bu programlar yardımıyla uygun ikili ve üçlü kombinasyonlar sonucu belirli kompozisyonlara karşılık tahmini gözenek değerleri belirlenmiştir. Bu programlar paketlenme tahminleri için Dinger-Funk denklemini kullanmaktadır. Belirlenen komposizyonlardan hazırlanan karışımlar preslenip sinterlendikten sonra peletlerin yoğunluk ve gözenek ölçümleri yapılmıştır. %100

süper-öğütülmüş alumina toz içeren pelet 1550°C'de %98 teorik yoğunluğa ulaşmıştır. İnce taneli tozların oranının nispeten yüksek olduğu ikili ve üçlü karışımlarda peletlerin yoğunluklarının yüksek olduğu gözlenmiştir. SEA oranının %50'nin üzerinde olduğu ikili karışımlarda gözenek oranı artmıştır.

Ayrıca bu çalışmada ikili toz karışımlarında TiO_2 ve MnO_2 gibi ilave katkı malzemeleri kullanılmış ve katkı malzemelerinin yoğunlaşmaya ve malzemenin sertliğine etkileri incelenmiştir. Bu katkı malzemeleri peletlerin %91-99 arasında teorik yoğunluğa ulaşılmasını sağlamıştır.

Sinterlenen peletlerin mekanik özellikleri için sertlik değerleri ölçülmüştür. İnce taneli tozların oranının nispeten yüksek olduğu karışımlarda peletlerin Vikers sertlik değerleri 1500 ile 2100 $kg.mm^{-2}$ aralığındadır. Ayrıca, sinterlenen peletlerin ayrıntılı mikroyapısal karakterizasyonu SEM kullanılarak yapılmıştır.

Sonuçta, yoğunluğu ve sertliği en yüksek olan pelet baz alınarak istenen boyutlarda fayanslar üretilmiştir. Bu fayanslar için de yoğunluk ve gözenek ölçümleri, mikroyapısal ve mekanik karakterizasyonları yapılmıştır.

TABLE OF CONTENTS

LIST OF FIGURES

LIST OF TABLES

Chapter 1

INTRODUCTION

Alumina has played an important role in ceramic industry from the first clay pots used by ancient man to the advanced electronic substrates in today's computers. It is one of the highest volume inorganic chemicals sold in the world today. It is used in many applications, ranging from wear and ballistic applications to refractories industry. It is a dominant ceramic material not only because of its superior mechanical, thermal and chemical properties, but also because of outstanding electrical properties that make it excellent low-tension and high-tension insulator. The electrical properties make it adaptable for use in applications ranging from substrates for microelectronic applications to spark plug insulators. Also, it is widely used in applications such as dental ceramics in bio-medical areas, wear-resistant materials in textile industry, grinding balls and abrasives [1-5]. The utilization of low-grade alumina powders in ceramic processing to manufacture structural components, such as wear resistant tiles, sealants, o-rings and nozzles has always been desirable in industrial applications [6].

Alumina ceramics are low cost and can be manufactured using a variety of methods such as dry pressing, slip casting and injection molding, without the use of expensive equipments [5,7]. Also, they can be manufactured by using tape casting, extrusion, isostatic-forming methods [2]. They are often densified by solid-state sintering techniques [8].

Recently the utilization of alumina ceramics has increased in our country. The increasing area of the use of alumina ceramics has increased interest for evaluating of domestic Bayer alumina powders. As a result of this increase, it has become important to enhance the properties of low-grade alumina powders that are being produced as metallurgical grade at Seydişehir Aluminum Plant, so that it can be used in technical ceramic applications.

In this study, blending of SKA (Seydişehir Coarse Alumina), SEA (Seydişehir Electrofilter-residue Alumina) and Alcoa-CT3000SG alumina powders with three different types of particle size distributions was investigated to develop a dense alumina ceramic tile with desirable mechanical properties. MXENTRY and MIX10 softwares were employed for preparation of powder blends for maximum packing in the green

state. Software predictions were based on Dinger-Funk equation [9] that is quite similar to Andreassen's equation [10] for packing except for the presence of a finite size in the small particle end of the distribution. Additives like TiO_2 and MnO_2 were used for improved diffusion kinetics to maximize density.

This thesis contains the following subjects. In Chapter 2, a literature review of the production of alumina is given. In Chapter 3, packing of particles and software used for predictions are presented. In Chapters 4 and 5 the results obtained from this work are shown and discussed. Finally, in the last chapter the conclusions and recommendations for future work are given.

Chapter 2

PREPARATION OF ALUMINA CERAMICS

In this chapter, preparation of alumina ceramics from raw materials, their forming and sintering processes will be briefly presented.

2.1. Production of Bayer Alumina

Bauxite is a naturally occurring, heterogeneous material comprised primarily of one or more aluminum hydroxide minerals plus various mixtures of silica, iron oxide, titania, aluminosilicates, and other impurities in trace amounts. The principal aluminum hydroxide minerals found in varying proportions within bauxite are gibbsite ($Al(OH)_3$) and the polymorphs, boehmite and diaspore (both AlO(OH)) [2,11].

In 2002, World production of bauxite amounted to more than 144 million tons. In Turkey, Seydişehir Aluminum Plant has annual production capacity of 460,000 metric tons. World output of alumina amounted to about 51 million tons per year. Besides, in Turkey, 200,000 metric tons of alumina was produced. Today, more than 95 percent of the world's total alumina is produced from bauxite by the Bayer Technology [11-13]. Alumina, which is an intermediate product, is produced for the metallic aluminum and ceramics industries. The Bayer Process, an economical method of producing aluminum oxide, was discovered by an Austrian chemist Karl J. Bayer. In 1887, he published the patent for the decomposition of aluminate solution, and in 1892, he published the first patent for solubilizing the bauxite by addition of sodium hydroxide solution under high pressure and temperature. This patent presented the main principles of the Bayer method applied today [14,15]. This process was implemented for the first time in 1893, by the "pure alumina" company, in Gardanne (South of France), a setting close to both the bauxite and the coal that is necessary for the thermal supply [14].

The Bayer process consists of five steps;

a) Grinding of bauxite,
b) Digestion,
c) Settling (or clarification),

d) Precipitation of $Al(OH)_3$ from the solution by the use of nucleating agents,

e) Calcination.

The steps to produce metallurgical grade alumina are shown in Figure 2.1.

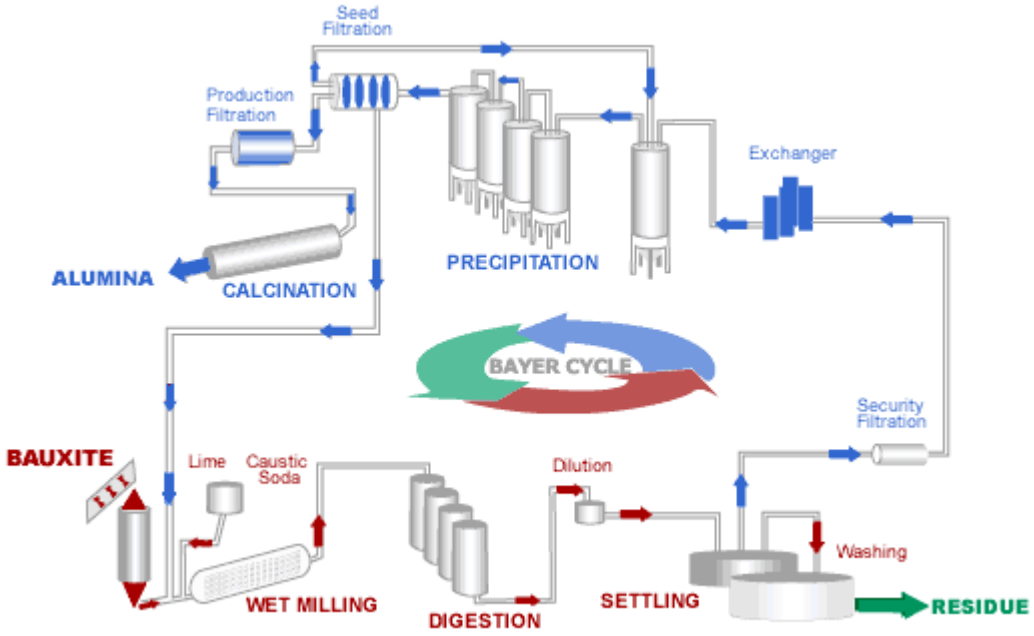

Figure 2.1. Schematic flow diagram of the Bayer process for alumina powder production [14].

The principal operations in the Bayer process are the physical beneficiation of the bauxite, digestion, settling (clarification), precipitation, and calcination followed by crushing, milling and sizing. During the digestion, most of the hydrated alumina goes into solution as sodium aluminate in sodium hydroxide (caustic soda) solution under a pressure of about 25-35 atmosphere and at a temperature of about 250°C, and insoluble compounds of iron, silicon and titanium which are called as "Red Mud", are removed by settling and filtration. The filtrated sodium aluminate solution is seeded with very fine gibbsite ($Al(OH)_3$) and at lower temperature the aluminum hydroxide reforms as the stable phase. The agitation time and temperature are carefully controlled to obtain a consistent gibbsite precipitate. The gibbsite is filtered and washed to reduce its sodium content and is calcined at 1100-1200˚C to obtain α-Al_2O_3. High-purity (up to 99.5%) alumina with a particle size ranging from several microns to submicron can be produced by this process [1,2,15-18]. Corundum, α-Al_2O_3, is a thermodynamically stable form of

aluminum oxide. Its excellent thermal, mechanical and dielectric properties make it one of the most important ceramic raw materials. It has hexagonal type of corundum structure and high melting point as 2050˚C [16]. In Table 2.1, physical and thermodynamic properties of α-Al_2O_3 are shown.

Table 2.1. Physical and thermodynamic properties of α-Al_2O_3 [19].

Phase	α - Al_2O_3
Crystal structure	Hexagonal
Lattice parameters (A°)	A = 4.758 C = 12.991
Entropy, $S°_T$ at 25 °C, (J/[kg-mol·deg])x10^{-3}	51.020
Standard heat of formation, $-\Delta H°_{298}$, (J/[kg-mol])x10^{-6}	1.675.557
Free energy of formation of oxides, -ΔF at 25°C, (J/[kg-mol])x10^{-6}	1.577.461
Specific heat capacity, C_p at 25°C, (J/kg·deg)	775
Heat of fusion, ΔH, (J/[kg-mol])x10^{-6}	108.86
Thermal expansion coefficient, (10^{-6} / °C) –200 to 25 °C 25- 200°C 25- 400°C	 3.4 6.5 7.4
Density (g/cm^3)	3.96-3.98
Melting point (°C)	2050

Five structures of hydroxide (trihydroxides and oxyhydroxides) exist in nature. Industrially, gibbsite, boehmite and bayerite can be synthesized. There are three crystalline forms of trihydrated alumina or aluminium trihydroxide – $Al_2O_3.3H_2O$ or $Al(OH)_3$. These are gibbsite (gamma-$Al(OH)_3$), bayerite (alpha-$Al(OH)_3$), nordstrandite (beta-$Al(OH)_3$). There are two crystalline systems of alumina, monohydrated or oxyhydroxide – $Al_2O_3.H_2O$ or Al(OOH). These are boehmite (gamma-Al(OOH)) and diaspore (alpha-Al(OOH)). Gibbsite is the most common synthetic form prepared from bauxite in the Bayer process. The sequence of transitions are shown graphically in Figure 2.2.

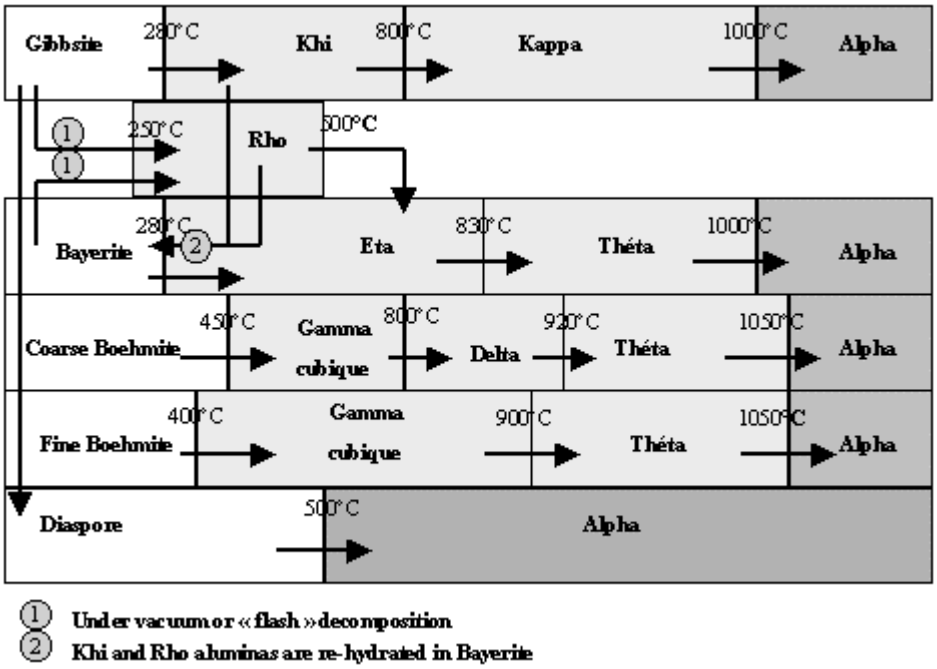

Figure 2.2. Dehydration sequence of Alumina Hydrates [14].

If the calcination temperature is lower than 1100˚C, metastable transition phases of alumina such as rho, chi, eta, epsilon, delta, theta, gamma, beta and kappa may occur. They are usually obtained in variable mixtures depending on the precursor and the conditions of preparation. More than 25 solid phases of alumina have been described in recent years, but it is doubtful whether some really exist. These phases or forms include amorphous hydrous and anhydrous oxides, crystalline hydroxides, and aluminas containing small amount of oxides of the alkalies or alkaline earths, designated as β-aluminas. These transition phases have poor sinterability and grindability. They also induce laminations, shrinkage and distortions in the final ceramic products [2].

Disadvantages of Bayer alumina:

a) Bayer alumina is produced by the use of copious amounts of sodium caustic (NaOH) solution.
b) Sodium is an undesirable element for mechanical and electrical properties due to the grain boundary glass promoting capacity for the former case and the presence of β-alumina for the latter case [20].
c) Therefore, such alumina must be cleaned before any further processing step is taken [21].

Presence of Na_2O in Bayer alumina has a significant effect on the conductivity or dielectric properties because it causes glass-phase formation at grain boundaries. The glassy phase along the grain boundaries also leads to inferior mechanical properties. In the literature, washing treatments had been applied to reduce alkali content of the powders in different solutions such as water and acids (HCl, H_2SO_4) and washing with water has given most suitable results [21,22].

Improvements in the quality of ceramic grade alumina have been made in two different paths: (1) the reduction of impurities in normal Bayer alumina, and (2) the development of particle size distributions having better packing properties [2].

2.2. Calcined, Reactive and Superground Aluminas

Commercial Bayer calcined aluminas are heated to obtain substantial amounts of α-Al_2O_3, the stable form of anhydrous alumina. The calcination of aluminium hydroxide can be carried out in three types of kiln: rotary kilns, fluidized bed kilns and tunnel kilns. Rotary kilns are the most suitable for the preparation of calcined aluminas. They have been perfected in many ways to reduce fuel consumption and to precisely adjust the size and the morphology of alpha alumina crystallites.

Although alpha alumina has a melting point of 2050°C, the relatively fine hexagonal crystal plates obtained during calcination permit sintering to occur at much lower temperatures. Shapes fabricated from some ground calcined alpha alumina powders have obtained 98% theoretical density at temperatures below 1450°C. Higher sintering temperatures improve thermal stability for refractory applications. Sintered and fused α-Al_2O_3 products made from calcined aluminas can provide all the advantages afforded by α-Al_2O_3; for example extreme hardness, resistance to wear and abrasion, chemical inertness, outstanding electrical and electronic properties, good thermal shock resistance and dimensional stability; and mechanical strength at elevated temperatures [16].

“Reactive” alumina is the term normally given to a relatively high purity and small crystal size (<1 μm) alumina which sinters to a fully dense body at lower temperatures than low soda, medium-soda or ordinary-soda aluminas. These powders are normally supplied after intensive ball-milling which breaks up the agglomerates produced after calcination. Thermally reactive aluminas were developed when dry

grinding aids permitted products containing submicron crystals to be dry ball milled to their ultimate crystals or superground. The grinding aids sorb on the surface of the alumina, prevent mill packing and reduce the energy required to separate the individual crystals from the Bayer agglomerates [16]. They are utilized where exceptional strength, wear resistance, temperature resistance, surface finish or chemical inertness are required [1]. These powders enabled 85, 90 and 95% Al_2O_3 ceramics to be upgraded to the higher alumina content with improved mechanical, thermal and electronic properties because they could be sintered without fluxes in the temperature range of about 1450-1750^oC [1,16]. The reactivity is improved so that fired densities of cold-pressed bodies (99.5% Al_2O_3) above 3.90 g/ml are attainable within one hour at 1500°C to 1550°C [2].

Superground alumina powders have a high purity (min. 99.8 wt% of Al_2O_3); the α-form content is 95 wt%. The average median particle sizes of the aluminas are 0.35-0.45 μm. The BET specific surface areas are 8-11 m^2/g [5].

2.3. Forming

Forming is the stage where ceramic powders are given the desired near net shape before densification. Several manufacturing processes are used commercially. The manufacturing processes include uniaxial pressing or dry pressing, cold isostatic pressing (CIP), slip casting, tape casting, roll compaction and extrusion [2,17,18,23]. Forming methods generally require additives such as binders. Binders are used to adhere ceramic particles to each other and to provide appropriate green strength for handling. Without a binder, green bodies are usually very fragile [18].

Among the many techniques for shaping ceramics, dry pressing and slip casting will be explained in more detail in this thesis. Because, these two techniques were employed in forming the powders in this study.

2.3.1. Dry Pressing

The simplest and most popular method of forming a ceramic shape is dry pressing. Dry pressing is the compaction of dry or slightly damp powders, usually with an organic binder, in a metal die at sufficiently high pressures to form a dense, strong piece. Dry pressing is a useful processing technique because it is inexpensive and can

form shapes to close tolerances and also, easily automated. This method is widely used in the ceramic industry to manufacture such components as ceramic tiles, spark-plug insulators, chip carriers, seal rings, valve components, refractories and other products of simple morphology [17,18,23]. For this method, the amount of binder used is in the range of 0.1 to 3 wt %. For example, polyvinyl alcohol (PVA) is a commonly employed hard binder used with many oxide ceramics. In dry pressing, PVA has a tendency to stick to the mold and usually necessitates a release agent for removing pressed parts. Green parts pressed with PVA are strong but brittle [18]. Applied pressures are commonly in the range of 3000 to 30,000 psi in this method [23].

2.3.2. Slip Casting

Slip casting is another method of manufacturing ceramic products that allows the formation of complicated shapes and designs without need for spray drying. The process of slip casting begins by filling a porous mold with a ceramic suspension. Water in the suspension escapes through the pores in the mold by capillary action, causing the ceramic body to solidify and form walls along the boundaries with the mold. The thickness of the solidified walls increases as time passes. When the desired thickness has been attained, the remaining liquid suspension is poured from the mold leaving the solid ceramic body behind. When the ceramic body has dried long enough to support itself, it is removed from the mold. Molds are often made up of multiple pieces, so the dried product may be easily removed. A common mold material for ceramic slip casting is gypsum [17]. Achieving a desirable slip necessitates close control of many parameters such as solid and additive fractions, particle size, pH, viscosity, mold properties, time, temperature and drying rate. Combining these parameters is critical for obtaining the optimum green density and strength in the cast body [18].

As a ceramic processing technique, slip casting has advantages and disadvantages. The advantages include a relatively low cost, a higher green density for the ceramic body, and the ability to form complex shapes. The disadvantages of slip casting include lower production rates and lower dimensional precision. Products that are often manufactured through slip casting include sanitaryware, whiteware, refractories, crucibles, porcelain items and closed-end tubes [17].

2.4. Firing

Ceramic parts that are formed by dry pressing or slip casting are dried at T>100°C and fired at high temperature to develop the ceramic bond within the material. The firing process provides the necessary driving force for diffusion, which facilitates bond formation between powder particles. The main function of sintering is reduction of surface area. Atomic scale transport is necessary for surface elimination. There are basically two methods for sintering: (1) Solid State Sintering and (2) Liquid Phase Sintering.

2.4.1. Solid State Sintering

Of the densification processes for high-modulus ceramics, solid-state sintering has been studied most. Relatively high-purity alumina ceramics are often densified by this technique [8]. Sintering may be defined as the consolidation, densification, re-crystallization and bonding of a ceramic body during firing, at temperatures below the melting point of the principal component [2,17,23,24]. Tammann rule states that sintering temperatures are usually ½ to 2/3 the melting point of the material at which diffusion processes can progress at appreciable rates.

During sintering, grains within the ceramic body join together to form larger grains. The microstructural surface area of the body decreases, decreasing the total surface energy in the body. Sintering does not necessarily result in densification of the body, but densification is suitable to improve strength [17]. In this process, powder compacts become dense by diffusional transport of matter through the solid, and densification steps can be illustrated by the idealized case of three spheres in contact, as shown in Figure 2.3 [8].

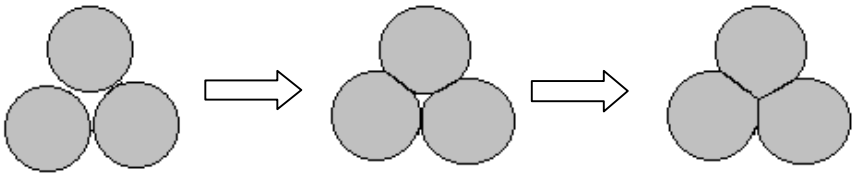

Figure 2.3. Solid-state sintering steps [8].

Solid-state sintering can be split into three stages as initial, intermediate, and final. The initial stage is a "neck growth" during which the particle surfaces are smoothed and interparticle contact area increases from zero to about 0.2 of the maximum cross-sectional area of the particles, and pores are rounded. So, a small amount of densification occurs. During the intermediate sintering stage, pores shrink through mass transport by neck growth. Grain growth begins, the pore phase is a continuous channel (tortuous) and all pores are intersected by grain boundaries. Pores shrink further and close during the final phase of sintering. In addition, smaller grains consolidate to form larger grains. The continuous pore phase becomes discontinuous. Preferably, at this stage, all pores remain on grain boundaries where their removal is kinetically favorable. However, it is more common for many of the pores to be isolated from the grain boundaries as a result of discontinuous grain growth, and this greatly impedes the attainment of full theoretical density. About 95 to 97 percent of theoretical density is considered adequate for most ceramics, for mechanical applications [8,17]. Recently it was suggested that grain growth could be helpful during the final stages of sintering to avoid pore/grain boundary separation [18].

The driving force for solid-state sintering is the tendency of particles to reduce their surface energies. There are, however, two alternatives that lead to surface energy reduction. These are grain growth (coarsening) without pore removal and densification with pore shrinkage. The force that causes the particles to merge together, the particles change shape to increase their contact area with neighboring particles, the voids that comprised the former interparticle spacing are driven toward free surfaces. The loss of voids during sintering results in volume reduction, and therefore, a density increase of the compact [8,23]. The rate and degree of densification as functions of time, temperature and pressure are important in sintering. Two key characteristics of solid-state sintering are overall shrinkage of the component and residual porosity [23,24].

The shrinkage of a compact is explained by the following equation.

$$\frac{\Delta V}{V_0} = 3\frac{\Delta L}{L_0} = 3\left(\frac{20\gamma a^3 D}{\sqrt{2}kT}\right)^{\frac{2}{5}} r^{\frac{-6}{5}} t^{\frac{2}{5}} \qquad (2.1)$$

Where $\frac{\Delta V}{V_0}$ and $\frac{\Delta L}{L_0}$ are the fractional linear and volume shrinkage, respectively, D is the diffusion coefficient, γ is the surface energy, a^3 is the atomic volume, k is the Boltzmann constant, T is the temperature, r is the particle radius, and t is the time. There

are many factors that can affect sintering rates. Some of the better-identified factors are temperature, pressure, atmosphere, impurity concentration, second phases, pore size distribution, and other initial microstructural features. The important parameters for sintering are temperature and surface area. When temperature increases, sintering rate increases. However, as a result of excessive sintering, materials tend to become weak with pore and grain growth. The sintering temperature may be reduced by introducing an additive to the system that either enhances the diffusion properties of the particles or improves diffusion by creating a small amount of a liquid phase during sintering. This sintering aid may be mixed with the system either as a solution or as a powder. One must take caution when adding a sintering aid because the introduction of a liquid phase during sintering affects the thermal and electrical properties of the final product [2,17,18].

An example of the densification behavior of a dense compact of a well-dispersed, nominally 1 μm magnesia-doped alumina powder during a constant rate of heating is shown in Figure 2.4.

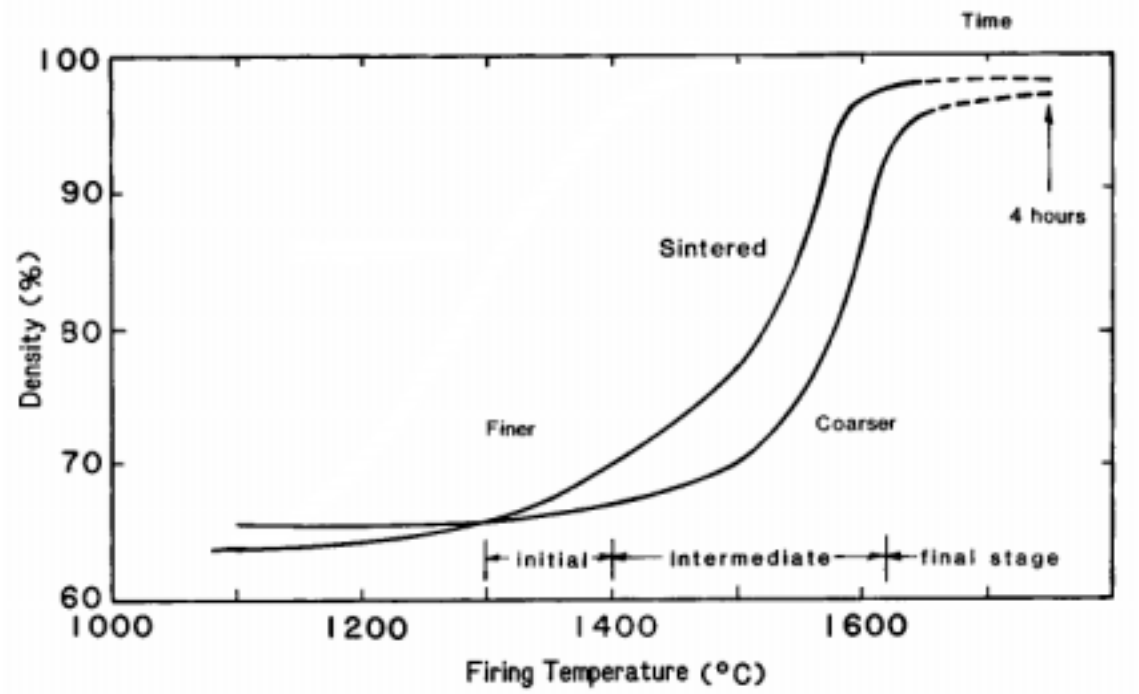

Figure 2.4. Densification behavior of compact of two alumina powders with a log-normal size distribution (d_M=1.3 and 0.8 μm) and the initial, intermediate and final stages of sintering for the coarser powder [17].

Sintering rate steadily decreases with time, so that merely sintering for longer periods to obtain improved properties is impracticable. Therefore, time is not a critical variable for process control. This case is illustrated in Figure 2.5.

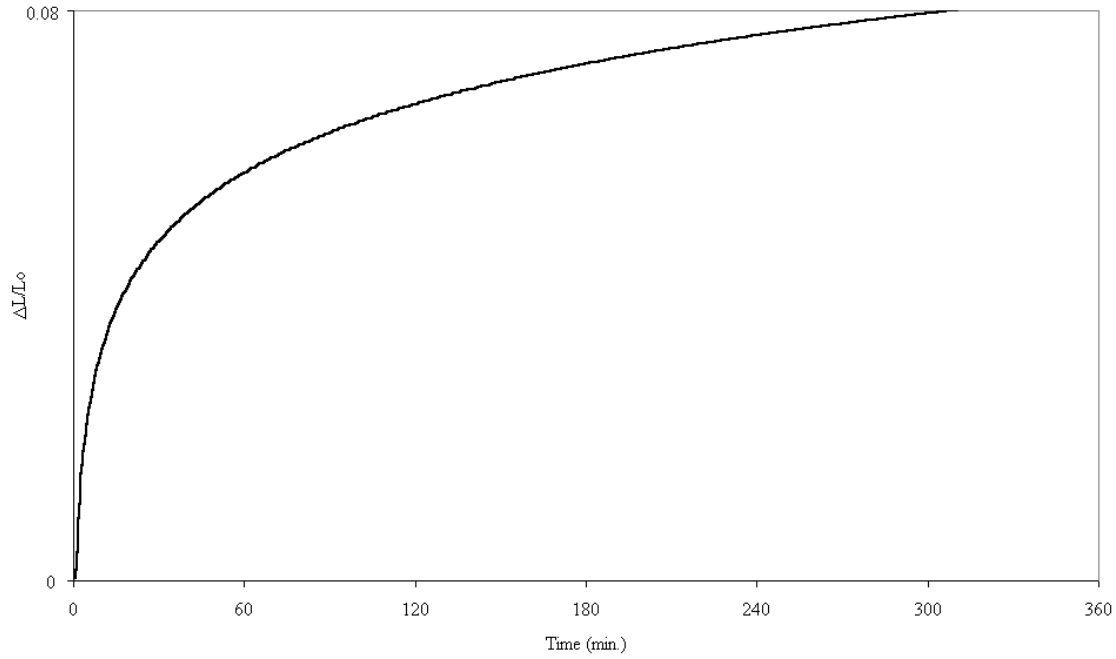

Figure 2.5. Effect of time on the shrinkage of alumina compacts [23].

One of the important aspects of sintering is to be able to control the growth of grains. Other than grain coarsening required to form a fully dense body, sudden excessive grain growth may occur due to grain boundary movement, when the hold time at sintering temperature exceeds the optimum. The rate of its growth increases exponentially with temperature. When the equilibrium dihedral angle between two grains of the solid and their surfaces is less than 60°, the interface between grains is convex and will tend to move outward, thus inhibiting pore closure. If the angle is greater than 60°, then the concave interface will allow pore shrinkage. For any one grain, the radius of curvature of a side is directly proportional to the grain diameter, so that the driving force, and therefore the rate of grain growth is inversely proportional to grain size by the equation below.

$$d^* = \frac{d(d)}{dt} = \frac{k}{d} \tag{2.2}$$

and integrating,

$$d_t^n - d_0^n = 2AM_b\gamma_b t \tag{2.3}$$

and

$$d - d_0 = (2k)^{1/2} * t^{1/2} \tag{2.4}$$

Where d_0 is the grain diameter at time zero and k is constant, A is the radius of the boundary, M_b is the mobility of the boundary, γ_b is the specific grain boundary energy and t is the time. n is a value between 2 and 4, and is depend on the temperature. This case is illustrated in Figure 2.6.

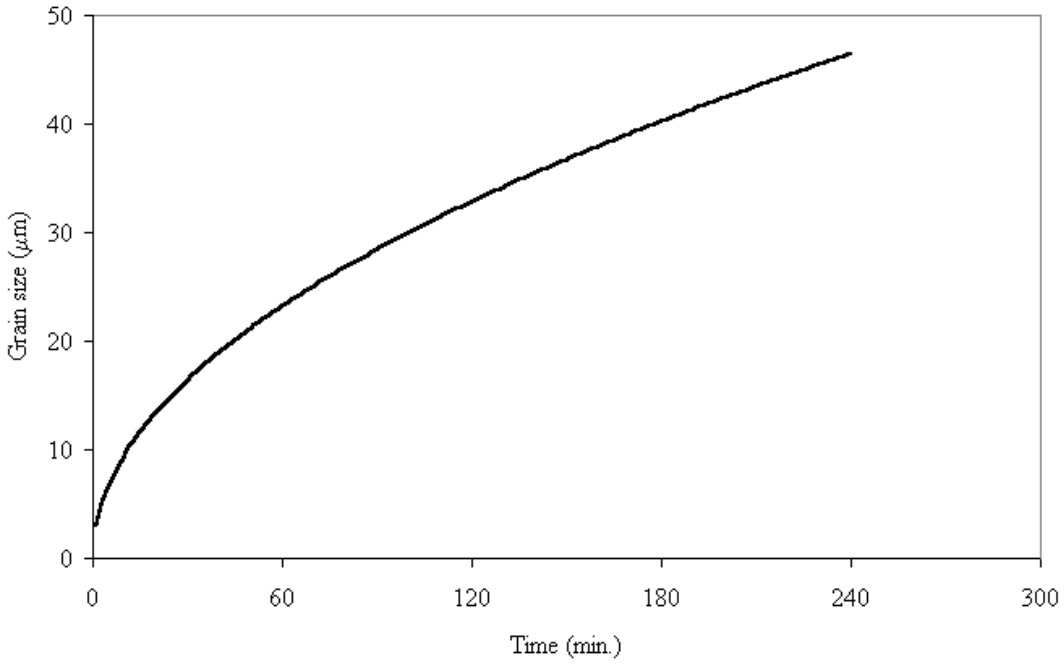

Figure 2.6. Grain diameter versus time for grain growth [23].

Control of particle size is very important, as the particle size is decreased; the rate of sintering is raised [23].

Defects in ceramic materials favor faster transport via enhanced diffusion [2]. Additives in the body create point defects. For example, effect of titania additions on the sintering rate of a relatively pure alumina works as follows. It is believed that Ti enters Al_2O_3 substitutionally as Ti^{+3} and/or Ti^{+4} (Ti_{Al}). The following reaction occurs:

$$Ti^{+4} + Al^{+3} = Ti_{Al} + V_{Al}^{\cdot}$$

$V_{Al}^{\cdot}$ means that a vacancy of aluminum is produced to maintain the charge neutrality in the system. Ti_{Al} term in Kroger-Vink notation is a titanium ion that is located on an aluminum site [23].

In summary, the conditions favorable for preparing ceramics of maximum density via solid-state sintering are:

a) Starting powders of very small particle size and high surface area,
b) Controlled additives like MgO or ZrO_2 to retard boundary mobility,
c) Uniform compaction of sufficient density,
d) Use of additives or furnace atmosphere that increases the lattice vacancy concentration [8].

2.4.2. Liquid Phase Sintering

Another common process for densification of high-modulus ceramics is sintering in the presence of a reactive liquid. For this sintering to occur, three criteria must be met. First, an appreciable amount of liquid must form at the sintering temperature. Second, the liquid phase must completely wet the solid phase, and third, the solid phase must be partially soluble in the liquid. Liquid phase sintering is an effective densification process for most high-alumina ceramics due to lowered sintering temperature and shorter sintering time. These materials contain 85 to 99 % alumina with alkaline-earth oxides and silica. At the sintering temperature, the components react to form a fluid liquid phase within the compact. On cooling, the liquid may completely crystallize or remain as an amorphous phase, depending on the cooling rate and the liquid composition.

Liquid phase sintering uses a liquid in the voids between particles to enhance sintering kinetics, and to affect the properties of the ceramic components. The pore-removal mechanism and the kinetics of densification for this sintering type occur in three steps.

a) Particle rearrangement,
b) Solution-precipitation,
c) Coalescence.

In the first step, the liquid is formed either by a eutectic reaction between different phases in the compact or by melting of one of them, and particle

rearrangement takes places under the influence of surface tension to give a more efficient particle packing. This rearrangement is one reason for the faster densification in liquid phase sintering as compared with solid state sintering. In the second step, densification proceeds by a solution of the solid material at contact points, diffusion through the liquid phase, and precipitation at solid surface sites outside the contact area. Because material transport by diffusion is more rapid in a liquid than in a solid, densification occurs at a faster rate in liquid phase sintering than in solid state sintering. In the third step, a solid skeleton forms in which the liquid phase will not penetrate the grain boundaries. This occurs when the energy of the solid-state interface becomes less than twice the energy of the solid-liquid interface. In general, the solid-solid interfacial energy decreases as the crystallographic misorientation of adjacent grains decreases [8,23].

2.4.3. Effect of Additives on Sintering

Main purpose of sintering is to provide densification without grain growth. Therefore, sintering agents are used to hinder grain boundary mobility. Additives have been used either as second phase forming agents or as a solid solution in alumina ceramics for several purposes. In both cases, the aim is to enhance the densification and suppress the grain growth. Formation of a liquid phase by using an agent within the body provides a rapid diffusion pathway to enhance densification. Additives as solid solutions not only enhance densification but also inhibit the grain growth by lowering the boundary mobility. Also, they are used to accelerate crystal growth, to accelerate sintering or shrinkage rate, to reduce firing temperature, to change pore shape, for changing the physical and chemical properties, and to remove impurities [2].

Crystal growth in sintered alumina is an unfavorable factor affecting strength and thermal shock resistance. Therefore, in ceramic bodies additives such as SiO_2, Cr_2O_3, CaO, MgO and ZrO_2 are used [2,3,5,6]. Addition of MgO to alumina, have been found to slow boundary migration, and allow complete pore elimination by solid state sintering [3,5,23]. Titania is known as an effective additive to densify alumina below the firing temperature. TiO_2 addition stabilizes the lattice defects in corundum at different temperatures [2]. Addition of MnO_2 doped alumina provides a uniform and dense microstructure at higher temperatures. Recently, effects of these additives have

been investigated on microstructure and mechanical properties of alumina ceramics [25,26].

Chapter 3

PACKING OF PARTICLES

In this chapter, an introduction to fundamentals of particle packing and a computer software that is used for particle packing calculations, are presented. The software that is explained in the second part of this chapter was used in this thesis for prediction of percentage porosities of different particle compacts.

3.1. Fundamentals of Packing of Particles

The packing of particles has always been of interest to ceramists because a good packing particle compact will fire to higher densities. Such increases in densities result from reduction of diffusion distances and attainment of a larger number of particle-to-particle contacts. When the resulting fraction of pores within the fired product are small, the mechanical properties of material will be improved due to the presence of small amount of flaws in the material and an increased load bearing cross-sectional area. Therefore, it is important that ceramics are formed from well-packing mixtures of particles.

The two foundation works on packing of particles were made by Andreassen et.al. [10] and Furnas [27]. An extensive literature review on packing is provided by Dinger et.al. [9]. Other important contributions to the subject came from McGeary [28], Westman et.al. [29] and Fuller et.al. [30] who worked on different materials ranging from nuclear fuel pellets to concrete aggregate sizing.

Furnas's work deals with discrete particle size distributions (PSD) for the packing of discrete particles sizes [27]. He states that best packing occurs when finer particles exactly fill the space within the larger particles. When the size classes are three, the finest particles must fill the void space within the medium sized particles which themselves fill the spaces between the larger sized particles. This can similarly be extended to distributions with n particle sizes. The size ratio of coarse to fine particles ideally should be infinitely large to optimize packing as was described above. In real systems, however, ratios like 20:1 or 10:1 are common. The larger the ratio the closer it

is to the theory that explains packing of discrete particles [27]. It is, on the other hand, difficult to produce perfect monodispersions to use in such systems.

Since monodispersions are difficult to achieve, most of the studies deal with discrete size classes like one bounded by adjacent sieves. The fraction of complete PSD that is bounded between two sieves is in fact a continuous distribution but it is nevertheless the closest we can get to a monodispersion in process systems.

Another contribution to particle packing came from Westman and Hugill who developed an algorithm that used discrete theory of packing [29]. They demonstrated a procedure for mixtures of two and three different sizes and gave an algorithm for higher number of size classes.

McGeary proposed a discrete approach to packing of particles that were used as nuclear fuel pellets [28].

Andreassen's work [10], however, constitutes the basis for continuous PSD where all particle sizes are shown on a distribution like in Figure 3.1. His first paper appeared in 1930 in which he evaluated existing work at that time on packing. Upon review of literature at that time he mentioned Furnas's work [27] and Fuller's work [30] that explained packing in concrete mixes he concluded that an appropriate packing theory should be one developed specifically for continuous distributions. Andreassen [10] described the theoretical considerations leading to the derivation of his equation from dimensional analysis and geometry. He used granulation images of particles of two neighboring size classes. Irrespective of the magnification the same image was observed that led him to the PSD equation for particle packing:

$$\frac{CPFT}{100\%} = \left(\frac{D}{D_L} \right)^n \tag{3.1}$$

where CPFT : Cumulative percent finer than the size D

D : Particle size

D_L : Largest particle size

n : PSD modulus (usually n = 0.3 – 0.5)

The above equation is the most widely used equation in the literature for packing of particles. Andreassen also confirmed the validity of his equation via experimental tests and concluded that the distribution modulus, n should be between 1/3 and 1/2.

Such equations are also interestingly encountered in discussions of fractal geometry, where similarity conditions are also common [9].

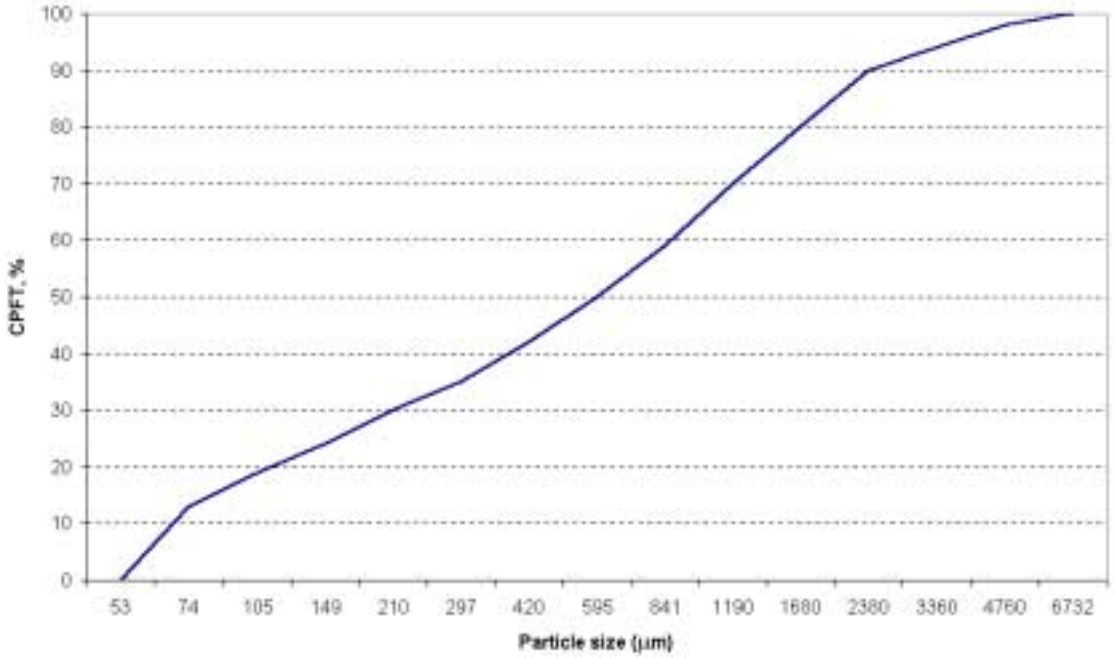

Figure 3.1. A typical continuous particle size distribution (PSD).

Dinger and Funk later recognized that there should be a smallest particle size for packing equation of Andreassen [9]. Therefore, they came up with the following equation:

$$\frac{CPFT}{100\%} = \frac{D^n - D_S^n}{D_L^n - D_S^n} \tag{3.2}$$

where D_S^n is the size of the smallest particle. Andreassen's and Dinger-Funk's (DF) distributions are compared in Figure 3.2 where bending of the CPFT curve for DF distribution at small particle sizes differs from the classical straight line of Andreassen's equation. Real powders analyzed for distributions are well known to show this type of bending. Hence, DF equation is closer to real distributions. In many discussions on packing of real particles, however, Andreassen's distribution provides a good fit. An

example is the packing of refractory ceramics which have a large size difference between neighboring size classes.

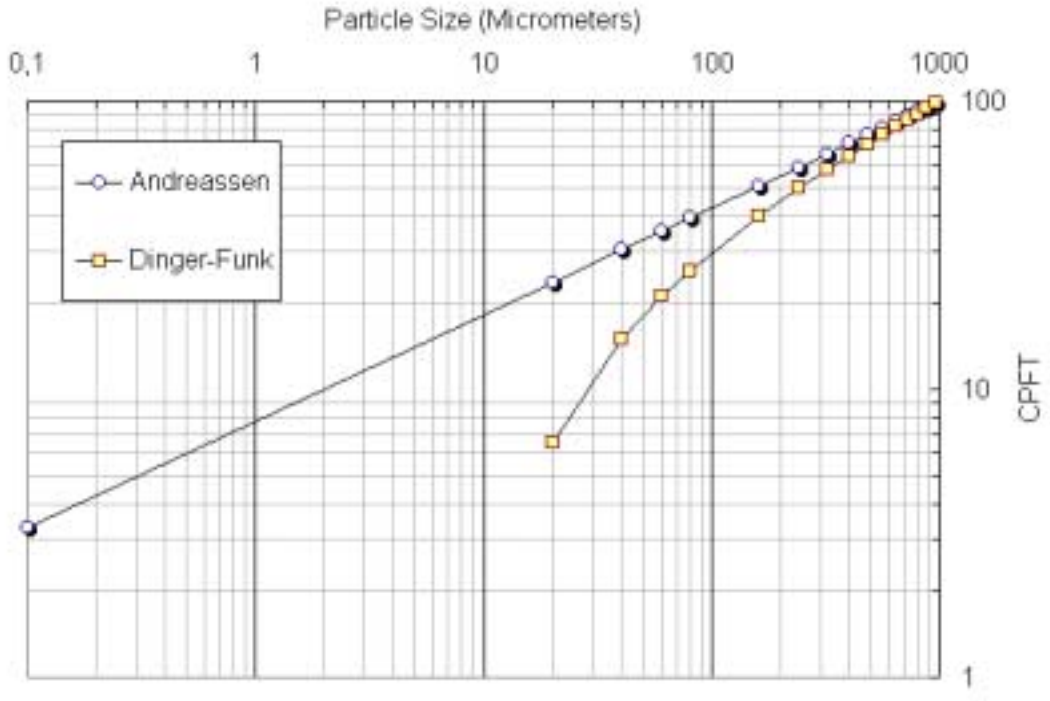

Figure 3.2. Andreassen and Dinger-Funk (DF) PSD with n=0.37 [9].

3.2. Computer Programs Used For Powder Packing

Dinger and Funk later developed a series of computer programs called MXENTRY and MIX10 that run on MSDOS. These programs that run on MSDOS platform, were developed to calculate particle packing parameters [9].

3.2.1. MXENTRY®

MXENTRY® is a program that allows the user to create MX-files from experimental PSD like sieve analysis. MX-files use a standard format that contains the parameters listed in Table 3.1. Column labels are at the bottom of each column in Table 3.1. The first two lines of the data file contain miscellaneous data and results for the material represented in the file. The first line starts with a label. It is followed by the calculated specific surface area (SSA) and the calculated total number of particles in a true cubic centimeter of powder (PCI). Next are the surface area shape factor (SF) and

the methylene blue index (MBI). The second line of the data file contains the number of entries in the PSD (38, for example) followed by the D_L (the largest particle size), D_S (the smallest particle size) and n (distribution modulus) parameters for DF distribution that best fits the distribution contained in the data file. These three parameters and the sum of squares term (which indicates whether the fit is good or not) are only present if the MXLSQ least squares fitting program has been run for the particular data file. The main body of each data file contains 8 columns. CPFT data as a function of D (particle size) are entered into the software which eventually calculates the resulting % in class, surface area (cm^2/g), cumulative surface area, calculated porosity, number of particles in class and cumulative number of particles. The program can also calculate the predicted values of the above parameters based on (i) DF equation, (ii) Andreassen's equation and (iii) log normal distribution. A shape factor (SF) must be entered into the software before any analysis is performed. This number is selected from Table 3.2. which is computed based on geometrical considerations.

Table 3.1. Standard MX-file format [9].

Example One SSA=12.84214 PCI= .17987D+14 SF=2.62 MBI=3.00 38 LEAST SQS D_L= 29.000 D_S= .030 n= .0800 SUM SQS= .23495430E-02							
.170	20.09						
.202	22.44	2.35	1.99050	12.84	12.68	.703D+13	.180D+14
.241	24.94	2.50	1.78532	10.85	12.99	.446D+13	.110D+14
.286	27.46	2.52	1.50790	9.07	13.66	.266D+13	.649D+13
.340	30.09	2.62	1.32197	7.56	13.93	.165D+13	.383D+13
.	.	.	.	.	.	.	.
.	.	.	.	.	.	.	.
.	.	.	.	.	.	.	.
62.118	99.25	.30	.00081	.00	32.46	.305D+05	.612D+05
73.892	99.51	.26	.00061	.00	34.65	.161D+05	.307D+05
87.896	99.79	.27	.00054	.00	36.10	.100D+05	.146D+05
104.555	100.0	.21	.00034	.00	40.00	.456D+04	.456D+04
Size (μm)	CPFT	% in Class	Surface Area in class	Cumula-tive SA (m^2/g)	Calculated Porosity	# in class	Cumulative # in PCI

Table 3.2. Surface area shape factors (aspect ratios = L/t) [9].

Sphere		1			
Tetrahedron		1.48			
Octahedron		1.37			
Square Disks	(31.62)/1	4.40	Hexagonal	(39.24/1)	4.38
	(9.72/1)	2.44	Disks	(13.88/1)	2.41
	(2.83/1)	1.41		(3.51/1)	1.37
Cube	(1/1)	1.24		(1.24/1)	1.18
	(1/2.83)	1.38		(1/2.28)	1.30
	(1/11.19)	1.93		(1/9.01)	1.80
	(1/61.65)	2.66		(1/25.51)	2.47

3.2.2. MIX10®

Once a PSD is entered into the computer by using the MXENTRY software further analysis like blending of different powders can be performed virtually on the computer by the use of MIX10 software. This program uses the Dinger-Funk (DF) methodology to calculate expected porosities and packing efficiencies. A new MX data file is created for the resulting blend. The program runs on MSDOS operating system and is a freeware program.

Chapter 4

EXPERIMENTAL PROCEDURE

In this chapter, first the raw materials, the pre-treatments to improve the raw material quality such as hot washing and re-calcination, and methods used for analysis are presented. Secondly, the techniques used for particle size distribution (PSD) analysis of powders are described. Later, the computer programs used for prediction of maximum packing of the powders and preparation of the mixtures are presented. In the last part, forming processes and firing of the tile followed by product analysis are explained.

4.1. The Raw Materials

In this thesis, three different types of alumina were used. The first one was a coarse metallurgical grade Bayer alumina (SKA) from Seydişehir Aluminum works, while the second one was again obtained from Seydişehir plant but from a different location within the process. It was an under sieve fraction of an electrofilter (SEA). The third type of alumina was a reactive grade superground Alcoa product (CT3000SG). The physical and chemical properties along with microscope images of these materials are given in detail in Chapter 5.

Seydişehir Coarse Alumina (SKA): The type of alumina is metallurgical grade alumina powder with certain impurities from the Seydişehir Aluminum Plant in Turkey. The powders have coarse particle sizes and their chemical analysis, physical properties and PSD are given in Table 4.1. These powders have about 15% α-Al_2O_3 content, because they were partially calcined for dehydration of $Al(OH)_3$. Also, these powders include high amount of sodium oxide.

Seydişehir Electrofilter-residue Alumina (SEA): The other type of alumina used in this project was again a metallurgical grade alumina powder with certain impurities from the Seydişehir Aluminum Plant in Turkey. This powder was named Electrofilter-residue Alumina and coded as SEA. In Seydişehir works, during calcination of the powders, when aluminum hydroxide is burned with fuel oil, the fine

powders are airborne and are collected by electrofilters. Therefore, the color of these powders is gray due to the high amount of carbon contamination. Also, this powder has a high level of sodium oxide contaminant [15].

Table 4.1. Chemical analysis, physical properties and sieve analysis of original Seydişehir Coarse Alumina (SKA) powders [31].

Chemical Analysis	
Al_2O_3 (%)	98.5 min.
SiO_2 (%)	0.02 max
Fe_2O_3 (%)	0.025 max.
Na_2O (%)	0.5 max.
Physical Properties	
Absolute density, (g/cm^3)	3.3-3.6
Loss of Firing (1100°C) (%)	1 max.
α-Al_2O_3 content	15 % min.
Sieve Analysis (Tyler)	
+100 Mesh	3-10 %
-100 Mesh +200 Mesh	25-40 %
-200 Mesh +325 Mesh	30-50 %
-325 Mesh	15-30 %

Superground Alumina (Alcoa CT3000SG): The last type of alumina powder used in this thesis was a commercial alumina. This powder was a reactive, superground alumina. Published properties of these powders are given in Table 4.2. Also, their particle size distribution (PSD) is shown in Figure 4.1.

Table 4.2. Chemical analysis and physical properties of Alcoa CT3000SG Alumina powder [32].

Chemical Analysis and Physical Properties	
Al_2O_3 (%)	99.76
Na_2O (%)	0.08
Fe_2O_3 (%)	0.02
SiO_2 (%)	0.03
CaO (%)	0.02
MgO (%)	0.09
Specific Surface Area / BET (m^2/g)	7.0
Average Particle size, (μm)	0.7
Press Density / 90 Mpa (g/cm^3)	2.25
Fired Density / [1540°C/1h] (g/cm^3)	3.90
Shrinkage / [1540°C/1h] (%)	16.8

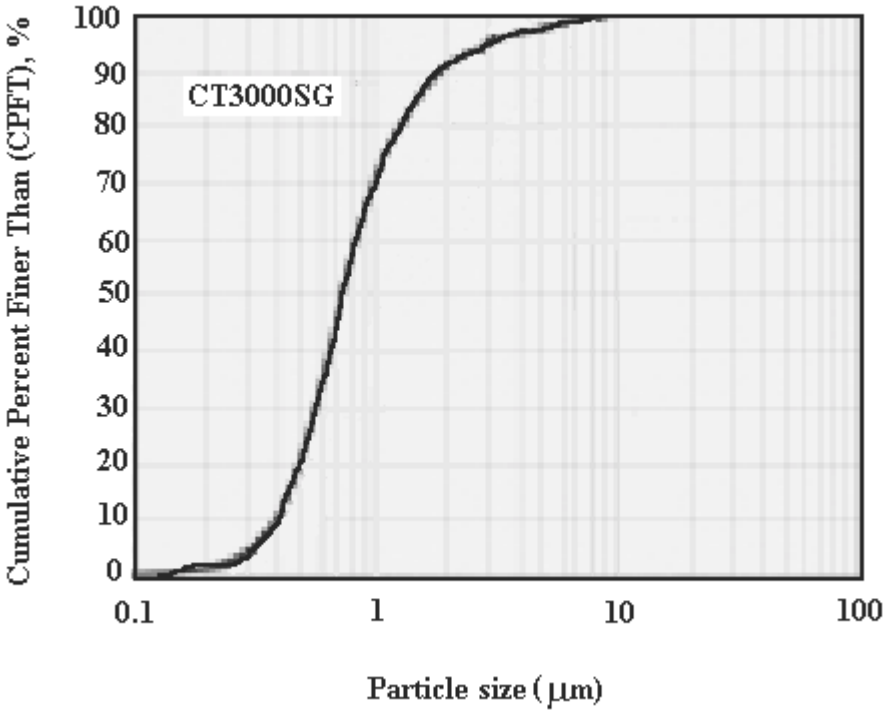

Figure 4.1. Typical particle size distribution of Alcoa CT3000SG alumina powder [32].

4.2. Pre-Treatment Studies

Domestic Bayer alumina powders need pre-treatments to improve their quality to use as a ceramic material. Therefore, these powders were subjected to a few pre-treatments. Quality of the powders can be improved with a variety of methods such as washing, calcination, and grinding. The raw materials can be purified from impurities such as sodium oxide by a simple washing technique. Washing operations are generally made with solutions such as water and some acids. In the literature, Mistler et.al. [21] reduced the sodium content of alumina powders fourfold by washing with distilled water. Washing treatment with water is mostly preferred for large-scale production at low cost. Other treatment to improve the powder quality is calcination, which is done to increase α-phase content. Another treatment is grinding which reduces the particle size.

Washing treatments: This treatment is the first step to improve the quality of domestic Bayer alumina powders.

Washing operations of SKA powders were initially done with deionized water and some acids such as HNO_3, HCl, and H_2SO_4. In this study, 0.2 grams of as-received SKA powder was washed in 0.1 M (25 ml) acid, and deionized water at 30°C for 28 hours at a mixing speed of 150 rpm in a stirred water bath (GFL-1092). This first treatment was only applied to SKA powders.

The second washing treatment was applied to both SKA and SEA powders. In this treatment, only hot water was employed. Seven hundred fifty (750) grams of as-received alumina powder was stirred in a container with two liters of deionized water on a heater for one hour. Temperature was controlled with a thermometer at about 95°C. The washing treatments were repeated five times. After washing, the powders were filtered with filter paper. The filtered cake was dried in an oven at 110°C for 18 hours and was analyzed by AAS and ICP for alkali content.

Re-Calcination: Another treatment to improve the powder quality is calcination. After washing, the domestic Bayer alumina powders (SKA and SEA) were calcined at 1250°C for one hour in order to convert γ-Al_2O_3 into the α-phase and to reduce the carbon content of SEA. Phase analyses of calcined powders were done by using X-Ray Diffraction device (XRD, Philips X-Pert Pro).

4.3. Chemical Analysis of the Powders

Chemical analysis of the powders that were subjected to the pre-treatments were realized at four steps, as follows:

1) Fusion operations,
2) Dissolution in acids,
3) Preparation of standard solutions of the elements,
4) Na, K and Ca analysis.

0.1 grams of powder (as-received and pre-treated SKA and SEA) along with one gram of flux (Lithium tetraborate) were fused in platinum crucibles at 980°C for one hour in an electric benchtop kiln. The fused fluxes were dissolved in 1.61M (100ml) dilute acid (HNO_3, HCl and H_2SO_4) while being magnetically stirred on hotplate. Besides, standard solutions of the elements were prepared to constitute their calibration lines that are between 1 to 3 ppm. Multielement (23-elements) standard solution was used for Na, K and Ca elements. Elemental analyses for Na, K and Ca were done by Atomic Absorption Spectroscopy (AAS-Thermo Elemental Solaar M) and Inductively Coupled Plasma-Atomic Emission Spectrometer (ICP-AES, Varian Liberty Series II).

4.4. Pre-Grinding

50 grams of domestic Bayer alumina powder was partially dry ground in a 250 ml tungsten carbide pot by the planetary mono mill (Fritsch Pulverisette 6) with thirty tungsten carbide balls (Ø: 10 mm) used as the grinding media. Dry grinding was applied at 300 rpm for 3 hours. A photograph of the ball mill is shown in Figure 4.2.

Figure 4.2. Photograph of the Planetary Ball Mill (Fritsch Pulverisette 6).

4.5. Particle Size Distribution Analysis

The size distributions could be determined by quantitative measurements of microstructural images. There are accepted methods such as lineal intercept method widely used to measure the grain size of cross-section of metallographic specimens and powders [33-36]. In this study, for particle size distributions (PSD) of the unground and ground powders we used the lineal intercept method.

Review of the Lineal Intercept Method: The lineal intercept method established by Heyn in 1903. By this method, the mean grain size can be calculated from the number of grains (intercepts) or grain boundaries (intersections) that intersect one or more random lines of known length superimposed on a field of view or micrograph. In lineal analysis, one drawn across a micrograph is used, and fractional length intercepting each particle size is measured. This can be done manually or with an integrating stage micrometer. The method also gives a distribution of intercepts. Because the measurements are made in only one dimension, no assumption of the shape of the particle is made. Particles were, however, not acicular or needlelike but were close to spherical shape. Equation 4.1 correlates the equivalent grain diameter to the intercept count:

$$d = L \times \frac{A}{M} \text{ , and } L = \frac{L_L}{N_L} \tag{4.1}$$

where d is the equivalent grain diameter, L is the mean intercept length, L_L is the fractional length intercepting each particle size along the line, N_L is the quantity of intercepts along the line, M is magnification (dimensionless) and A is the shape correction factor.

From relatively simple methods of lineal analysis, the volume fraction and surface area of particles and their size distribution can be determined. From a histogram of the mean intercept lengths, a calculation of the particle size distribution for three-dimensional microstructural features can be made. All particles are assumed to have the same (quantitative) particle shape [33].

In general, the analyses are based on the assumptions that the grains have spherical shapes and that the distribution of grain sizes can be represented by a discontinuous distribution. Provided that the class intervals are not too large, the greatest errors in results would be expected to arise from deviations of the grains from spherical shapes. This is not too bad an assumption for equiaxed grains or convex particles. In every case, however, a major practical problem is the detection and measurement of the smallest grains. If only a few of the smallest grains are missed, negative values of the number of particles may be obtained for these sizes.

Application of the Lineal Intercept Method: In this analysis, the three images for each one of unground and ground powders were obtained at the same magnitudes by using SEM. Ten lines were randomly drawn on each micrograph. The length intercepting each particle was measured and the mean intercept length was calculated. During calculation of the mean particle size, the shape correction factor was taken as 4/3 [34]. For each specimen, the histogram of the particle size distribution (PSD) was plotted. The results are given in Chapter 5.

4.6. Preparation of the Powder Mixtures

After particle size distribution (PSD) of each powder was determined, the MXENTRY software was used to predict maximum packing combinations of the three

powder mixtures. The new MX data files for each powder were obtained from their class size data versus CPFT data, which are experimental data, entered at the keyboard. Once the MX files were created, MIX10 program was ready to calculate the compositions of the blends that will pack most densely in the green state. Several different mixtures of the three powders were blended on the computer, and the lowest calculated porosity values and their corresponding compositions were plotted. Four different types of blends were prepared:

1) In the first-type of blends, the ternary compositions for unground domestic powders (SKA and SEA) and CT3000SG powders were prepared in 10-gram batches. A mixture of 5 wt.% polyvinylalcohol (PVA) was added as a binding agent. The blends were well mixed with ethyl alcohol in an agate mortar. The mixed cakes were dried in an oven at 110°C for one hour and then uniaxially pressed. These blends were labeled as TU (Ternary Unground) for ternary compositions that contained the unground powders.

2) The second-type of blends contained ternary compositions of dry ground domestic powders (SKA and SEA) and CT3000SG powders. These blends were labeled as TG (Ternary Ground) for ternary compositions that contained the ground powders.

3) The third-type of blends were composed of binary mixtures of dry ground SEA and CT3000SG powders. These blends were labeled as BG (Binary Ground) for binary compositions that contained the ground powder.

4) The fourth-type of blends were composed of binary mixtures of dry ground SEA and CT3000SG powder with 3 wt% TiO_2 and MnO_2 additives. These blends were labeled as BGA (Binary Ground with Additives) for binary compositions that contained the ground powder with additives. In these blends, titanium (IV) oxide (d=3.9, 99+%, Aldrich) and manganese chloride tetrahydrate ($MnCl_2.4H_2O$, min. 99.0%, Sigma) were used as sintering additives. The manganese chloride tetrahydrate was dissolved in water to yield 3.0 wt% manganese oxide. The blends of alumina were gradually added to this solution while being stirred. The suspension was continuously dried in an oven at 110°C and agglomerates were crushed in an agate mortar. Non-oxide additives were decomposed into oxide at 600°C in the furnace. 3 wt.% titanium oxide was added into the blends, and well mixed by ethyl alcohol in an agate mortar. The mixed cakes were dried in an oven at 110°C for one hour. The dried cakes were crushed again in an agate mortar. The blends were then prepared for pressing.

4.7. Forming

Samples were shaped by two techniques: (1) slip casting and (2) dry pressing. The latter was, on the other hand, adopted due to the speed and ease of application.

(1) Slip Casting: For slip casting of alumina tiles a suspension, which is a mixture of 630 grams of alumina and 200 ml of deionized water, was prepared. The slip contained 76 wt% solid. First, alumina powders were gradually added and stirred with a mechanical mixer (Heidolph RZR 2020) at 150 rpm. During stirring, 0.5 wt% Darvan-C deflocculent was added in the suspension to prevent agglomeration. The dispersed suspension was poured into the gypsum mold (85mm x 85mm x 25mm). After about 30 minutes the green tile slightly shrank and was carefully removed from the mold. It was then dried at room temperature for one day and in the oven at 110°C for 2 hours. The tile was fired at 1550°C for one hour.

(2) Dry Pressing: All blends were uniaxially compacted in the hydraulic press (Yıldız Hidrolik-15 tons) under a pressure of 100 MPa (30 bar) in the stainless steel die (diameter: 12mm) in the shape of pellets.

The rectangular-shaped tiles (85mm x 85mm x 20mm) from 100 % CT3000SG alumina powder were uniaxially compacted in the hydraulic press (Hidrokar Hidrolik-100 tons) at a pressure of about 45 MPa (150 bar) in the steel die.

4.8. Heat Treatments

The sintering of the pellets and tiles were done at varying temperatures (1550-1650^{o}C) in the chamber-type high temperature furnaces (Protherm PLF 160/5-max.1600°C and Nabertherm HT-16/17-max.1700°C). The soak time was two hours and the heating rate was 10^{o}C/min.

Also, the thermal etching was applied to the polished surfaces of sintered samples at 1450°C for 22 minutes. A photograph of the furnace is shown in Figure 4.3.

Figure 4.3. Protherm PLF 160/5- High Temperature Furnace (Max. Temp.=1600°C).

4.9. Analyses of the Powders and Products

Surface Area Measurements: The surface areas of as-received domestic powders (SKA and SEA) were measured by BET method [36]. Nitrogen adsorption and desorption isotherms at 77K were measured using Micromeritics ASAP 2010 surface area analyzer. The powders were evaluated for surface area after degassing at 593K for 20 hours. Single point surface areas were calculated from the linear part of the Brunauer-Emmett-Teller (BET) plots. BET single point equation is

$$\frac{P}{V(P_0 - P)} = \left(\frac{1}{V_m}\right)\left(\frac{P}{P_0}\right) \tag{4.2}$$

Where V_m is monolayer volume (cm^3/g) and V is the quantity of gas adsorbed at pressure P. P_0 is the saturation pressure of the gas. V (total volume adsorbed) is measured at 77K (usually the boiling point of liquid nitrogen) for various values of P/P_0 (relative pressure is usually in the range 0.05-0.3). A plot of the left-hand side of equation against P/P_0 should yield a straight line with a slope ($1/V_m$). BET plot passes through the origin. The monolayer volume is then related to the surface area of the powder.

X-Ray Diffraction Analyses: The crystallinity and phase analyses of the as-received powders and the calcined powders were investigated by using X-Ray

Diffractometer (XRD-Philips X'Pert Pro) with Cu-K_α radiation (λ=1.54 A°) at 40 kV in the 2θ intervals of 5-70°.

Density and Porosity Measurements: The density and porosity of the sintered products were determined using Archimedes' technique (ASTM C 20-87) [37]. This method covers the determination of the following properties of sintered products: apparent porosity, water absorption, and bulk density. First, the dry weight of each sintered specimen taken directly from the kiln was weighed. Each test specimen was boiled for 2 hours in water. After boiling, each specimen cooled to room temperature while still completely covered with water, and immersed in water for a minimum of 12 hours before weighing. The suspended weight in water of each specimen was measured on the balance with Archimedes' apparatus (Precisa-XP220A). After determining the suspended weight, the specimen was wiped with a wet sponge to remove drops of water from the surface. The damp specimen was then weighed to determine its saturated weight. The density and other properties were determined based on these three weights.

Microstructural Analyses: The microstructural features of as-received powders and the sintered samples were determined using scanning electron microscope (SEM-Philips XL-30S FEG). Elemental analyses of as-received and calcined powders, and also the sintered samples were done using SEM-Energy Disperse Spectrometry (SEM-EDS). The morphological characterization of the grains and micropores were evaluated on polished and thermally etched sections. For microstructural analyses, sintered specimens were cut with a diamond saw, and were cold mounted in polyester. Samples were ground with silicon carbide papers and polished with diamond suspensions. Polished samples were removed from the mounts, and thermally etched at 1450°C for 22 minutes in globar kiln.

Analysis of Mechanical Property: The samples were analyzed for the mechanical property such as hardness. The Vickers microhardness values of the sintered products were measured using the Vickers microhardness tester (HVS-1000, Time Technology Europe) and the universal hardness testing machine with an optical unit (Zwick-ZHU2.5) by applied loads of 4.9N (for pellets) and 98N (for tiles) on polished surfaces. The average of five indentations from each specimen was recorded.

Chapter 5

RESULTS AND DISCUSSION

In this chapter, the results of work on ceramic pellets and tiles produced from mixtures of alumina powders with different particle size distributions (PSD) are presented. As mentioned in Chapter 4, as-received powders and improved powders were characterized. Also, PSD of the powders are plotted using lineal intercept method. The results of computer programs used for powder packing are also shown. Density and porosity measurements are evaluated. Moreover, the hardness measurements of the products are also presented and discussed.

5.1. Characterization of As-received Powders

Typical scanning electron microscopy (SEM) images of as-received Seydişehir coarse alumina (SKA) powders are shown in Figure 5.1. These figures show that shapes of SKA powders are close to spherical and the powders have coarse particle sizes with a broad range of particle size distribution (PSD) from sub-micron to bigger than 100 μm. The fundamental particle size was of course not this large owing to large agglomerates that formed during heating. This was also confirmed by the very high surface area of the same samples measured by the BET method (~124 m^2/g).

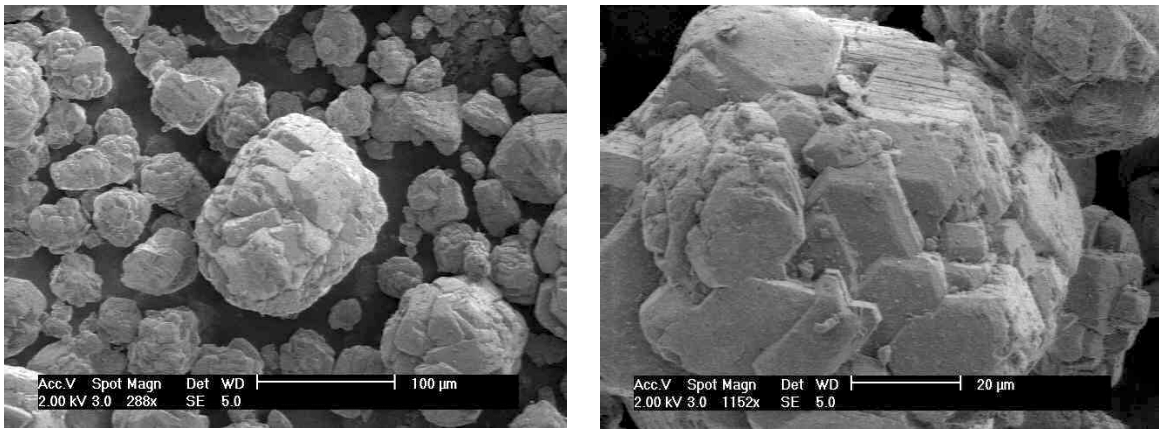

(a) (b)

Figure 5.1. SEM images at variety magnifications of as-received SKA powders.

The published PSD of as-received SKA powders was plotted as Tyler sieve opening in Figure 5.2. (The data was taken from Eti Aluminyum A.Ş. Product Catalog). According to this graph, average particle size of SKA was about 74 μm.

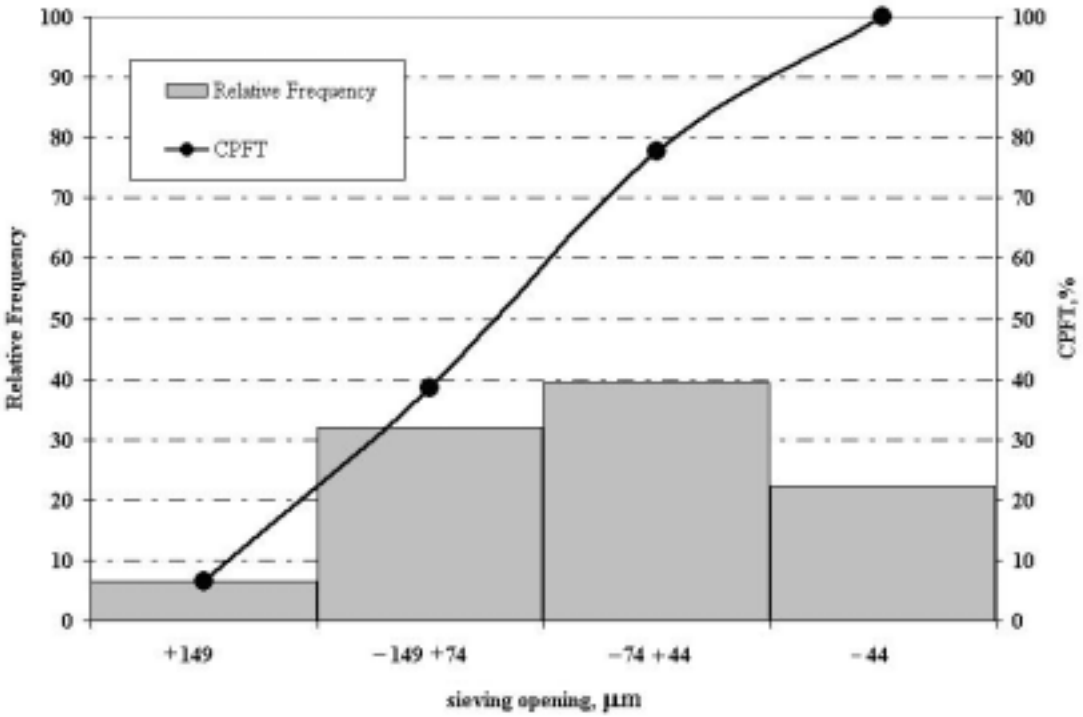

Figure 5.2. Particle size distribution according to sieve analysis of as-received SKA powders [31].

Typical SEM images of as-received Seydişehir Electrofilter-residue Alumina (SEA) powders are given in Figure 5.3. It can be seen that the shapes of the particles were close to spherical. The average particle size was smaller than 5 μm and the particles contained a large amount of tortuous pores.

Typical SEM images of Alcoa CT3000SG powders are shown in Figure 5.4. These figures showed that average particle size was smaller than 1 μm and that the particles were not as porous as the previous alumina powders.

BET specific surface area measurements of as-received powders were made using Micromeritics ASAP 2010 surface area analyzer. The powders were evaluated for surface area after degassing at 320°C for 20 hours. According to this, surface areas of the SKA and SEA powders were measured as 123.6 m^2/g and 22.2 m^2/g, respectively. Also, average pore diameters of the powders were measured as 7.4 and 4.4 nm, respectively. These results confirmed the previous finding that powder particles that

were pictured in SEM were not fundamental particles but were agglomerates formed from the fine particles. The fraction of tortuous pores was therefore significantly high in SKA and SEA.

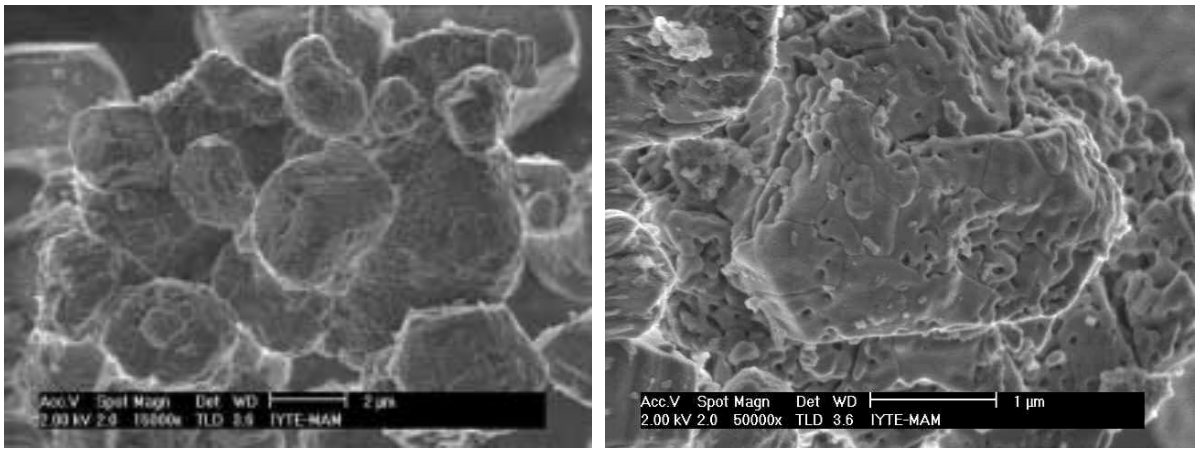

(a) (b)

Figure 5.3. SEM images at variety magnifications of as-received SEA powders.

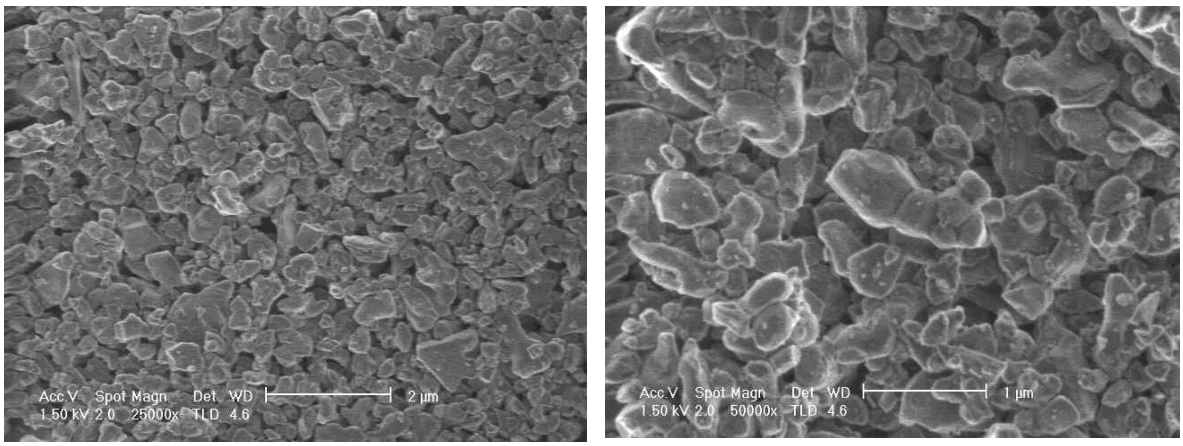

(a) (b)

Figure 5.4. SEM images of Alcoa CT3000SG alumina powders.

Crystallinity and phase analysis of as-received powders were investigated by XRD (Figure 5.5). According to the XRD chart, in SKA powders, γ-Al_2O_3 transition phase was observed together with α-Al_2O_3, due partially to their calcination during metallurgical-grade alumina production. In SEA powders, α-Al_2O_3 phase was dominantly observed. In Alcoa CT3000SG powders, α-Al_2O_3 phase accounted for all peaks in the XRD chart.

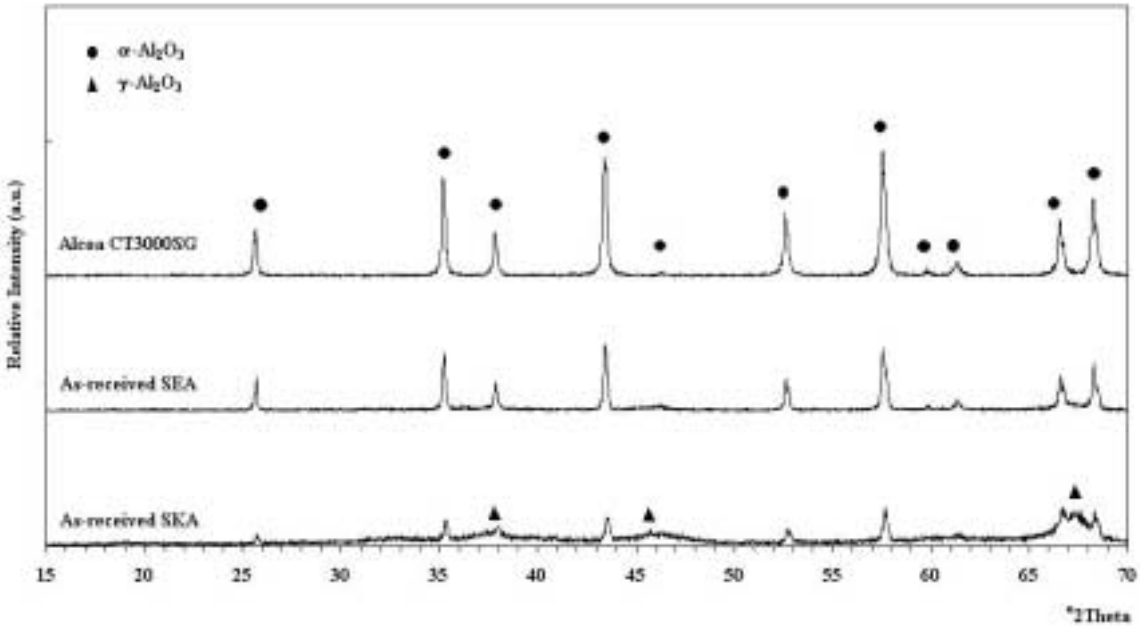

Figure 5.5. XRD graphs of as-received powders (Peak JCPDS reference numbers: α-Al_2O_3: 82-1399 and γ-Al_2O_3: 01-1308).

5.2. Characterization of Pre-treated Powders

Powders that were improved by washing, calcination and pre-grinding were characterized. SKA powders washed in acidic and water environments were analyzed by AAS the results of which are shown in Table 5.1. Sodium oxide (Na_2O) content of SKA powder treated with the acids and water are listed. Treatment with HNO_3 and HCl appeared to be more effective compared to H_2SO_4 and deionized water. The use of HCl brought the sodium oxide content down to 0.15%. The use of these acids for hot washing of alumina brought about problems in sodium analysis. Therefore, these acids were not used for treatment in later stages of the project.

Table 5.1. Na_2O content of the SKA powders treated with the acids and water (%).

Solutions (25ml)	As-received SKA powders fused	SKA powders washed at 30°C
0.1M HNO_3	0.33	0.2
0.1M HCl	0.34	0.15
0.1M H_2SO_4	0.35	0.3
Deionized water	-	0.25

Chemical analyses of SKA and SEA powders after hot-washing treatments with water are given in Table 5.2. The results show that hot washing is more effective. Hot washing with water provided low levels of sodium oxide. Na_2O content of SKA and SEA powders were reduced down to 0.11% and 0.25% from about 0.4% and 0.8% by hot-washing process, respectively.

Table 5.2. Chemical analyses of the SKA and SEA powders after hot washing with water (*: measured by using AAS; $^{+}$: measured by using ICP).

	SKA powders		SEA powders				
Impurities	As-received*	5 times washed*	As-received*	As-received $^{+}$	1 time washed *	1 time washed $^{+}$	5 times washed *
Na_2O	0.37	0.11	0.73	0.88	0.39	0.41	0.25
K_2O	0.04	0.03	0.14	0.27	0.08	0.21	-
CaO	0.14	0.11	0.14	0.18	0.09	0.12	-

Figure 5.6 shows XRD results of the calcined alumina powders. As a result of calcination at 1250°C for one hour, SKA and SEA powders were completely transformed into α-phase.

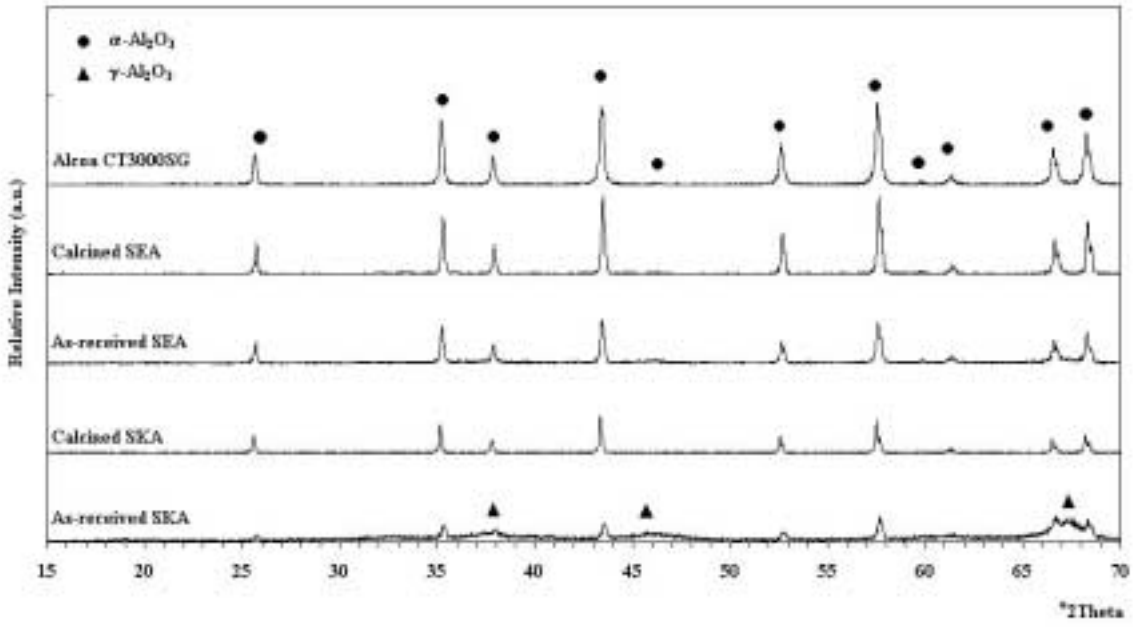

Figure 5.6. XRD graphs of the alumina powders that were calcined at 1250°C.

5.3. Results of the PSD Analysis by Lineal Intercept Method

Domestic alumina powders were partially ground. Particle size distributions (PSD) were reduced to suitable size intervals for better packing. The PSD data was generated using lineal intercept method. Measurements were made from three SEM images that were obtained at same magnification for each powder. Figure 5.7 (a) and (b) show SEM images of the unground and dry-ground SKA powders.

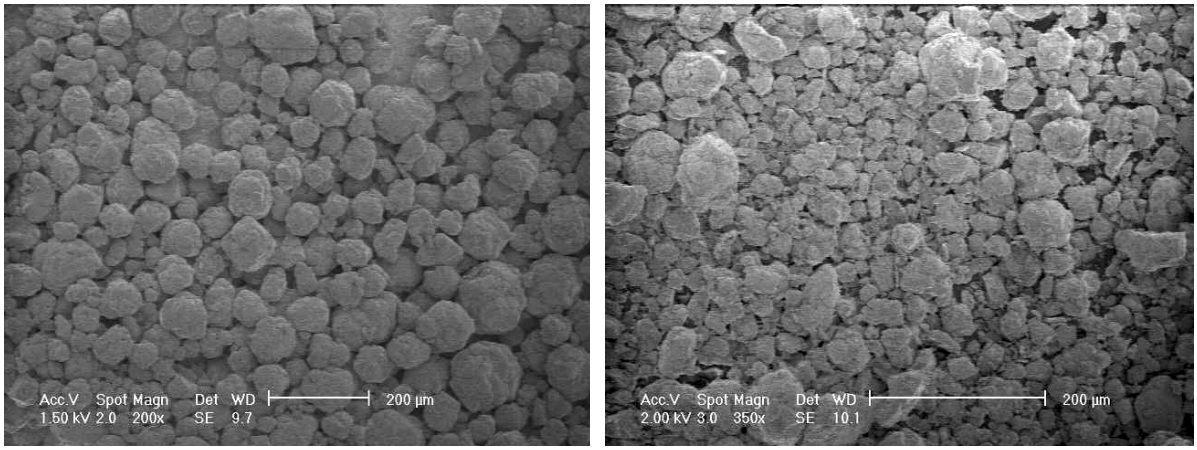

(a) unground SKA (b) dry-ground SKA

Figure 5.7. SEM images of 5 times hot-washed and calcined SKA powders.

Figures 5.8 and 5.9 show PSD graphs of unground and dry-ground SKA powders, respectively. 402 and 520 measurements were made from three SEM images for the unground and dry-ground powders, respectively. The result of PSD analysis of the unground SKA powders showed that the mean size was about 65 μm. After dry grinding, PSD of the SKA powder was mostly reduced to smaller than 30 μm.

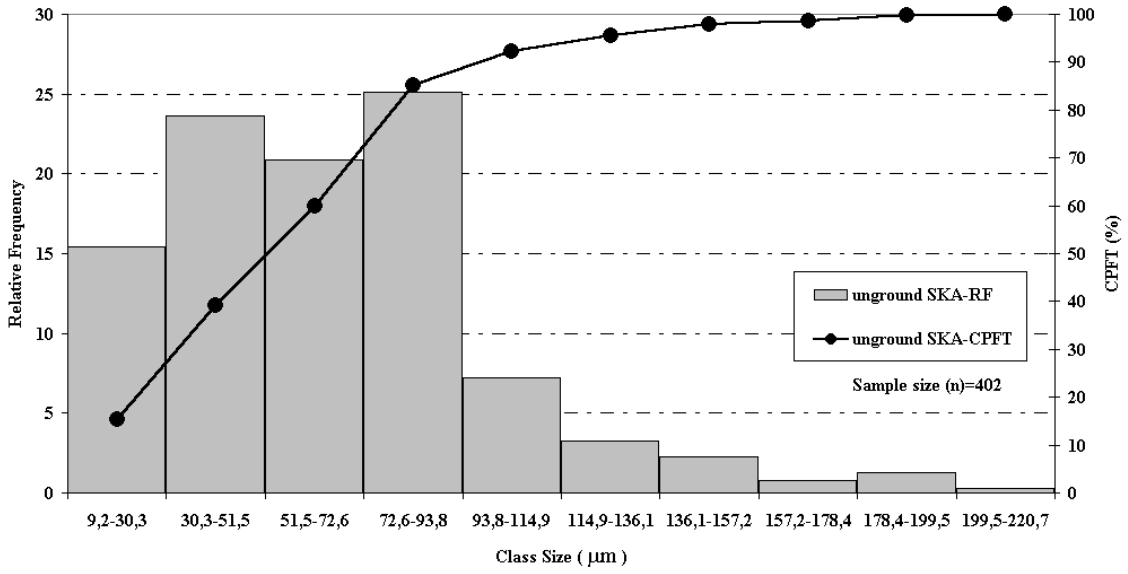

Figure 5.8. PSD histogram based on lineal intercept method of unground SKA powders.

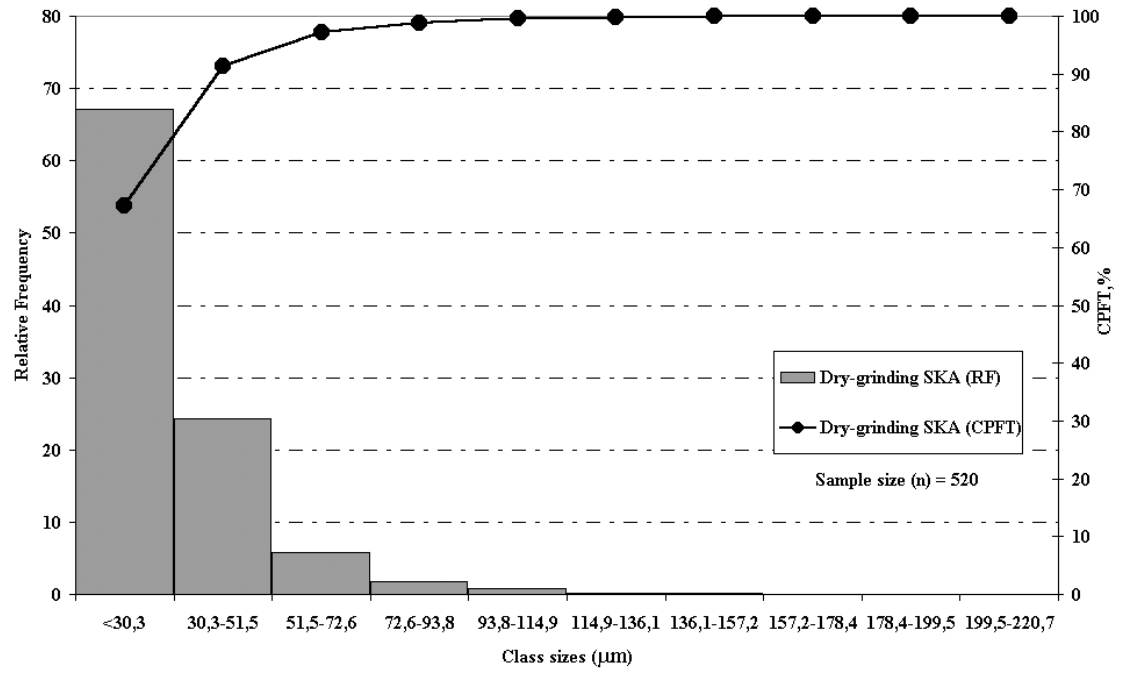

Figure 5.9. PSD histogram based on lineal intercept method of dry-ground SKA powders.

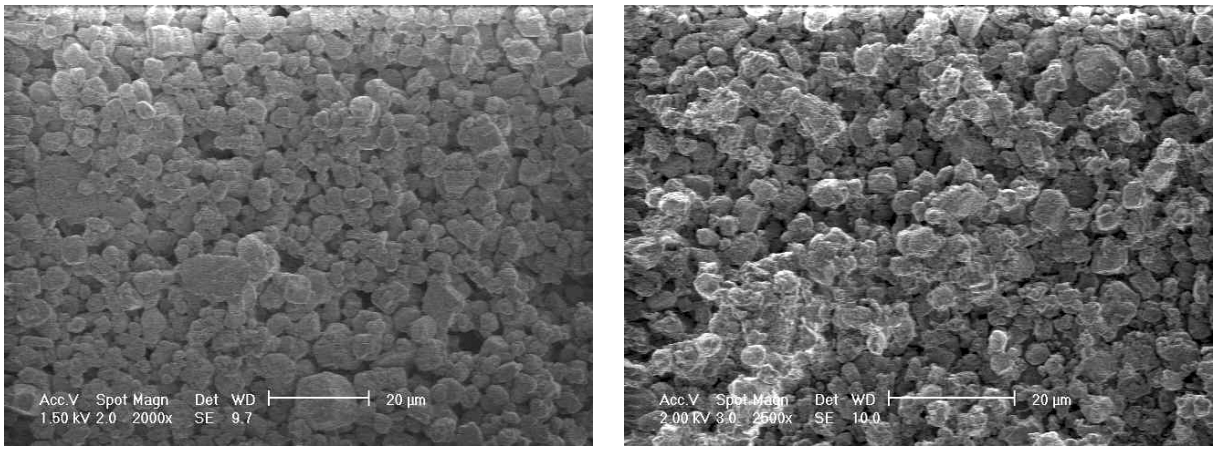

(a) unground SEA (b) dry-ground SEA

Figure 5.10. SEM images of 5 times hot-washed and calcined SEA powders.

Figure 5.10 (a) and (b) show SEM images of unground and dry-ground SEA powders. Figures 5.11 and 5.12 show the PSD graphs of these powders, respectively. 517 and 554 measurements were taken from three SEM images for the unground and dry-ground powders, respectively. The results of PSD analysis of the unground SEA powders show that the mean size is about 4-5 µm. After dry grinding, PSD of the SEA powders was mostly reduced to smaller than 3.4 µm.

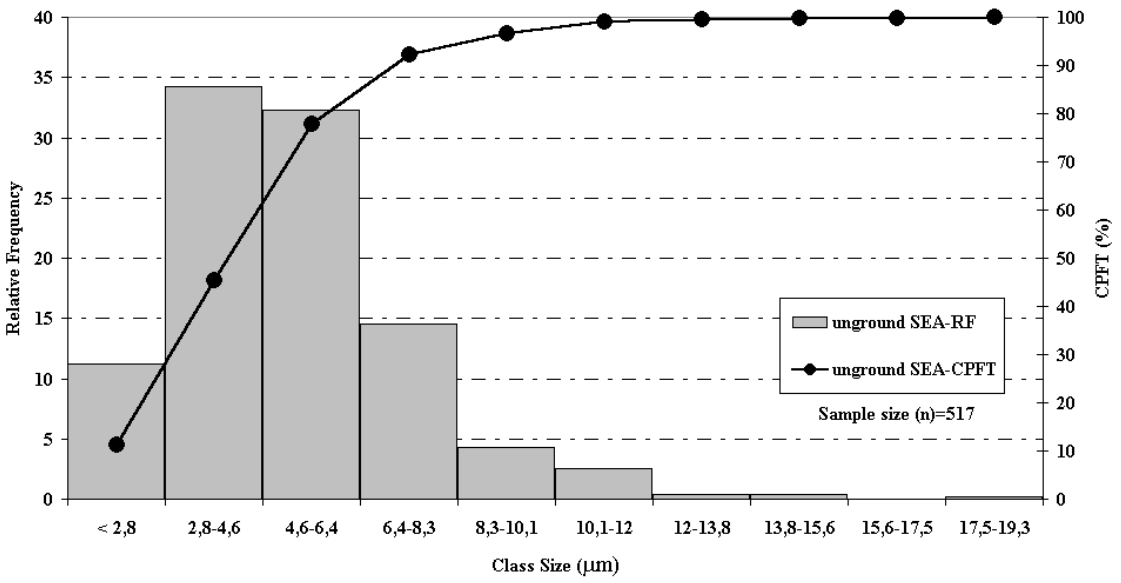

Figure 5.11. PSD histogram based on lineal intercept method of unground SEA powders.

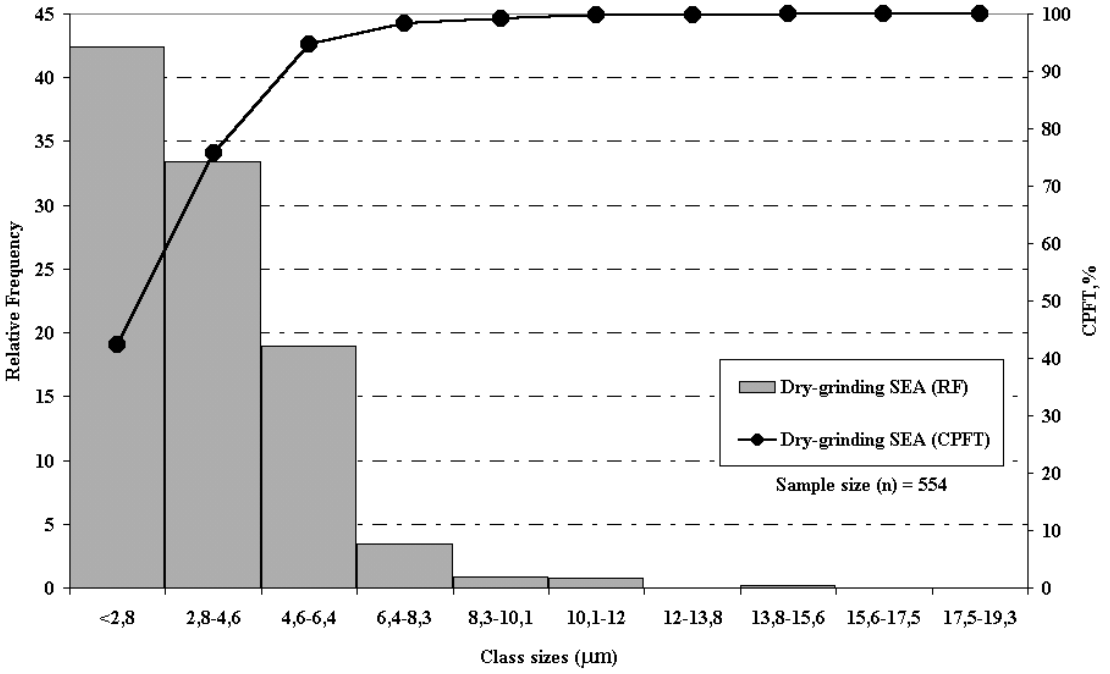

Figure 5.12. PSD histogram based on lineal intercept method of dry-ground SEA powders.

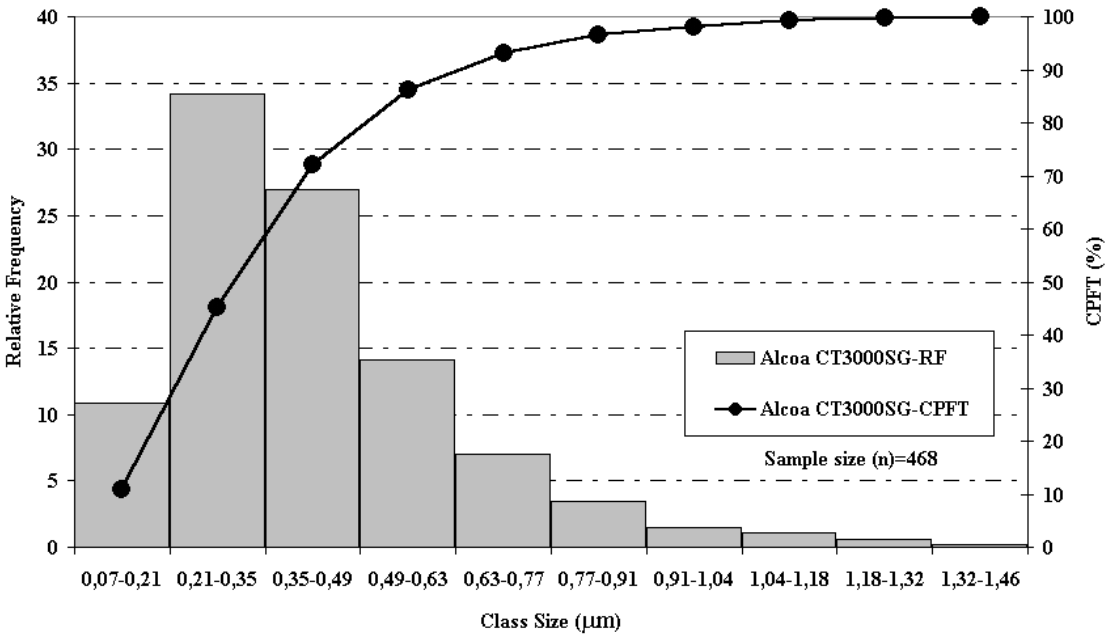

Figure 5.13. PSD histogram based on lineal intercept method of Alcoa CT3000SG powders.

Figure 5.13 shows the PSD graph of Alcoa CT3000SG powders. For PSD of these powders 468 measurements were taken from three SEM images. The result of

PSD analysis of the powders shows that the mean size is about 0.4 μm. This result was in agreement of the published average particle size of 0.7 μm (min. 0.5 - max. 0.8).

5.4. Results of the Computer Programs used for Powder Packing

MX computer software (MXENTRY ® and MIX10 ®) was used to predict the green density of powder compacts (TU, TG and BG) packed from a variety of blends of unground and ground powders. In this chapter, the computational results are presented.

5.4.1. Packing of Ternary Blends of the Unground Powders (TU)

For packing, the PSD data (class size data versus CPFT data) of the powders were entered into MXENTRY program. This program created the new MX data files of the powders. The data files contain a PSD histogram, surface area, cumulative surface area, calculated minimum porosity, number of particles, and cumulative number of particles for each particle size class. New MX data files of the unground SKA and SEA powders and Alcoa CT3000SG powders are given in Appendix A, respectively.

The MIX10 routine allowed us to mix the three powders stored in the MX data files. This routine calculated the lowest porosity values, and the compositions of the TU-blends (ternary blends of unground powders) required to obtain densest packing of the powders as given in Table 5.3. For this study, the calculated four TU-blends were prepared as shown in Figure 5.14.

Table 5.3. The predicted porosity and compositions prepared to obtain densest packing of the TU-blends using the MIX10 program.

Blends	Porosity, %	Distribution-1, % (unground SKA)	Distribution-2, % (unground SEA)	Distribution-3, % (Alcoa CT3000SG)
TU-1	12.63	50	29	21
TU-2	25.55	14	4	82
TU-3	27.95	0	100	0
TU-4	27.33	0	0	100

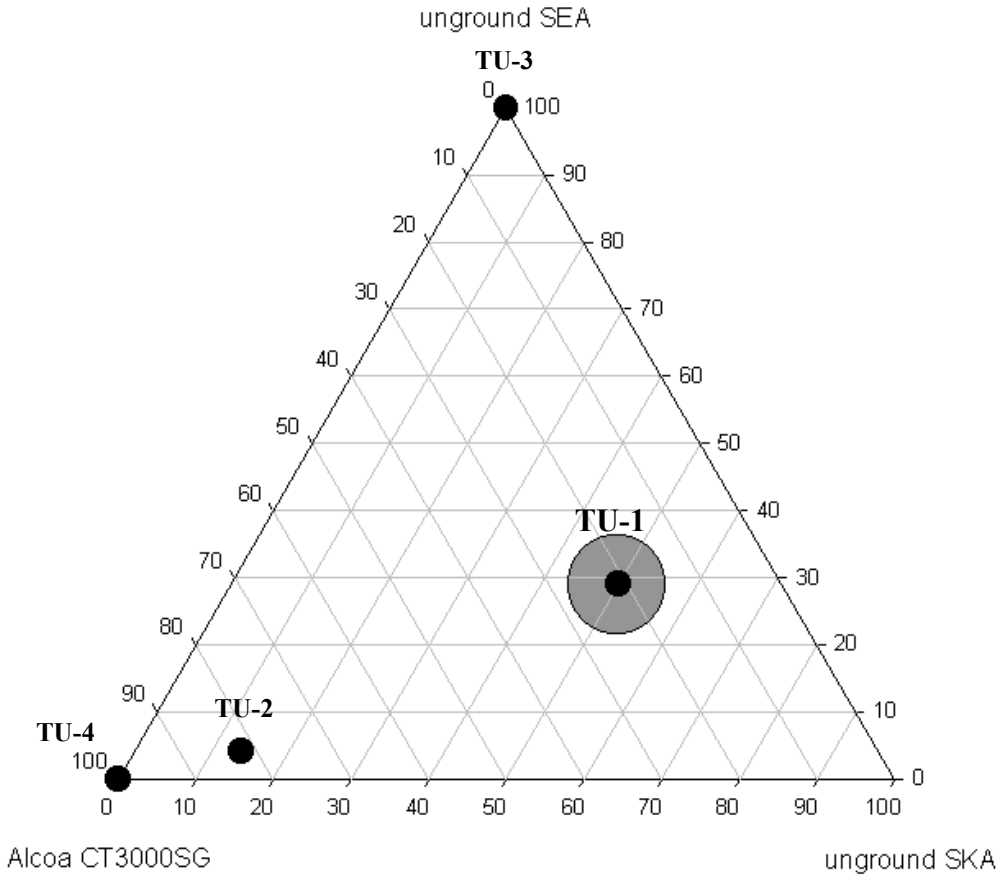

Figure 5.14. The blends prepared from unground powders (TU).

In Figure 5.14, TU-1 blend (painted area) had the least porosity value predicted which was about 13 %, and the maximum packing density was predicted to occur in this point. Also, the green packing density of these TU-blends was predicted to increase from about 72% to about 87%. These TU-blends were sintered at 1550°C and 1650°C for two hours. The density and porosity results of sintered pellets are given in section 5.5.1.

5.4.2. Packing of Ternary Blends of the Ground Powders (TG)

In order to further increase packing of powder blends, the two metallurgical grade powders (SEA and SKA) were ground at 300 rpm for 3 hours in a planetary mill. The MX data files of the ground powders are given in Appendix B, respectively. The MIX10 routine allowed blending the ground powders and Alcoa CT3000SG powders.

The predicted porosity corresponding to compositions of the TG-blends (ternary blends of ground powders) are given in Table 5.4 for 25 different blends.

Table 5.4. The predicted porosity and compositions prepared to obtain densest packing of the TG-blends using the MIX10 program.

Blends	Porosity, %	Distribution-1, % (ground SKA)	Distribution-2, % (ground SEA)	Distribution-3, % (Alcoa CT3000SG)
TG-1	22.57	20	20	60
TG-2	25.33	10	10	80
TG-3	25.33	20	0	80
TG-4	27.22	20	40	40
TG-5	28.87	35	30	35
TG-6	29.07	0	50	50
TG-7	29.77	25	50	25
TG-8	31.00	5	60	35
TG-9	31.34	45	40	15
TG-10	31.48	30	60	10
TG-11	32.21	50	0	50
TG-12	32.21	50	25	25
TG-13	32.21	50	50	0
TG-14	32.91	55	10	35
TG-15	33.28	10	80	10
TG-16	33.40	20	80	0
TG-17	33.50	60	20	20
TG-18	34.43	70	10	20
TG-19	34.54	0	100	0
TG-20	35.13	80	0	20
TG-21	35.13	80	10	10
TG-22	35.13	80	20	0
TG-23	36.10	100	0	0
TG-24	27.33	0	0	100
TG-25	33.50	60	10	30

In Figure 5.15, TG-1 blend (shaded circle) had the least porosity value predicted which was about 23% and the maximum packing density was predicted to occur in this point. Also, the green packing density of these TG-blends was predicted to increase from about 64% to about 77%. These blends were compacted and sintered at 1550°C and 1650°C for two hours. The density and porosity results of sintered pellets (TG samples) are given in section 5.5.2.

Minimum porosity is commonly known to be achieved at 70% Coarse + 30% Fine + 1-5% Medium based on Westman and Hugill's algoritm [17,23,24]. In this study, however, best packing mixtures were observed away from the above stated area and closer to the fine-medium line.

This difference should not be taken literally because Westman-Hugill's approach assumes that coarse, medium and fine particles are monodispersions, not continuous distributions like in this study.

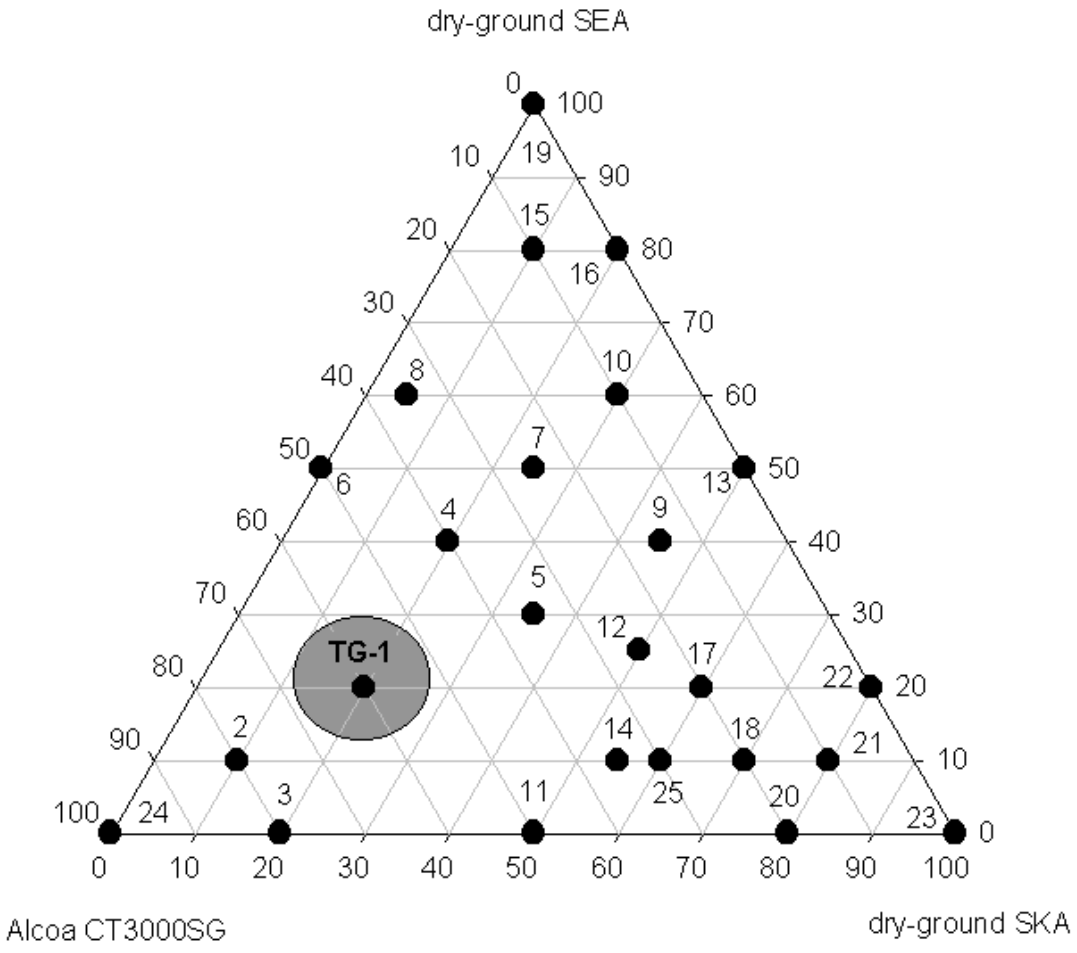

Figure 5.15. The blends prepared from ground powders (TG).

5.4.3. Packing of the Binary Blends (BG)

The MIX10 routine allowed blending the ground SEA and Alcoa CT3000SG powders for binary packing, and predicted porosity corresponding to the compositions of the BG-blends (binary blends of ground powders) are listed, and 11 different blends were prepared as shown in Table 5.5.

Table 5.5. The predicted porosity and compositions prepared to obtain densest packing of the BG-blends using the MIX10 program.

Blends	Porosity, %	Distribution-1, % (ground SEA)	Distribution-2, % (Alcoa CT3000SG)
BG-1	27.33	0	100
BG-2	26.4	10	90
BG-3	25.33	20	80
BG-4	24.06	30	70
BG-5	26.34	40	60
BG-6	29.07	50	50
BG-7	30.89	60	40
BG-8	32.19	70	30
BG-9	33.17	80	20
BG-10	33.93	90	10
BG-11	34.54	100	0

Table 5.5 shows that the BG-4 blend had the least porosity value predicted which was about 24% and the maximum packing density was predicted to occur in this blend. Also, the green packing density of these BG-blends was predicted to increase from about 65% to about 76%. These blends were compacted and sintered at 1550°C for two hours. The density and porosity results of sintered pellets without additives (BG samples), and with additives (BGA samples) are given in section 5.5.3 and 5.5.4, respectively.

5.5. Results of the Density and Porosity Measurements

The density and porosity results of the sintered samples from all ternary (TU and TG) and binary blends (BG and BGA) are presented in this section.

5.5.1. Ternary Blends of the Unground Powders (TU)

The results of the density and other measurements calculated by Archimedes' method of the compacted pellets from ternary blends of the unground powders (TU samples) sintered at 1550°C and 1650°C for 2 hours are given in Table 5.6.

Table 5.6. The results of the density and other measurements of the TU samples sintered at different temperatures.

Temperature, °C	Blends order	Apparent Porosity, %	Water Absorption, %	Bulk Density (g/cm^3)	Theoretical Density, %
1550	TU-1	33.4	12.6	2.65	67
	TU-2	9	2.5	3.53	89
	TU-3	26.9	9.5	2.84	72
	TU-4	1	0.3	3.84	97
1650	TU-1	28.8	10.3	2.81	71
	TU-2	3.7	1	3.69	93
	TU-3	-	-	-	-
	TU-4	0.6	0.2	3.87	98

It was observed that when the sintering temperature increased, fired theoretical density of the pellets increased. Consequently, the porosity and water absorption of the pellets decreased. The results show that the TU-4 sample achieved almost full density (98 %) at both temperatures. In the TU-1 sample, experimentally observed porosity values were higher than predicted porosity values. This was thought to result from the comparatively high shrinkage that occurred from the reactive Alcoa CT3000SG alumina. SKA powder contained tortuous pores that slowed down the shrinkage of the

compacts, leading to low densities. Therefore, the TU samples with a high amount of SKA will yield high porosity.

5.5.2. Ternary Blends of the Ground Powder (TG)

Results of density and other measurements (calculated by Archimedes' method) of the compacted pellets from ternary blends of the ground powders (TG samples) sintered at 1550°C and 1650°C for 2 hours are given in Tables 5.7 and 5.8.

Figure 5.16 shows the comparison of theoretical densities of the TG samples sintered at 1550°C and 1650°C. It was observed that when the sintering temperature increased, fired theoretical density of the pellets increased. This result was an expected result since an increase in temperature will produce better reaction and diffusion kinetics. Similarly, the porosity and water absorption decreased. As shown in Figure 5.16, samples that contained a relatively higher proportion of CT3000SG provided higher fired densities. Especially, the usage of 100% of this powder in the TG-24 sample achieved almost full density (98 %) at both temperatures. Because CT3000SG is a reactive alumina, its densification and shrinkage are higher than that of the domestic powders. Therefore, the TG samples that contained a relatively higher proportion of SKA have lower fired densities. If the proportion of SKA in total domestic alumina powders is up to 50%, densities of the TG samples decrease significantly.

Figure 5.17 shows the comparison of the porosity values predicted by MXENTRY in addition to the observed values for the TG samples sintered at 1550°C and 1650°C. As mentioned earlier, TG-1 sample packed to a porosity of about 23% as predicted, however, experimentally, it included 20% porosity after firing at 1550°C. When it was sintered at 1650°C, the fired porosity was reduced to 8%. As shown in Figure 5.17, observed porosity values of some samples were at comparatively lower levels. TG-2 and TG-24 samples achieved very low levels for both temperatures. These two samples provided the best two combinations as far as fired porosities are concerned. Also the samples coded TG-1, TG-3, TG-6 and TG-8 sintered at 1650°C, and TG-6 sintered at 1550°C had porosity levels lower than 10% which was roughly the limit for mechanical use of these materials. Moreover, as shown in Figure 5.17 observed porosity values of some samples was higher than predicted porosity values. These samples have contained a relatively higher proportion of coarse particle size distributions. This result

was not expected and probably resulted from the effect of inefficient mixing for predicted packing. Particles were probably unable to rearrange during sintering due to coarse agglomerate sizes.

Table 5.7. The results of the density and other measurements of the TG samples sintered at 1550°C for 2 hours.

Blends order (SKA/SEA/CT3000SG)	Apparent Porosity, %	Water Absorption, %	Bulk Density (g/cm^3)	Theoretical Density, %
TG-1 (20/20/60)	20	6.4	3.13	79
TG-2 (10/10/80)	8	2.2	3.62	91
TG-3 (20/0/80)	16.7	5.1	3.29	83
TG-4 (20/40/40)	22.5	7.5	3.01	76
TG-5 (35/30/35)	28.3	10.1	2.8	71
TG-6 (0/50/50)	12.5	3.6	3.43	87
TG-7 (25/50/25)	22.8	7.6	3.01	76
TG-8 (5/60/35)	17.2	5.3	3.23	82
TG-9 (45/40/15)	33.8	12.7	2.66	67
TG-10 (30/60/10)	31.3	11.4	2.75	70
TG-11 (50/0/50)	28.1	10	2.83	72
TG-12 (50/25/25)	33.7	12.9	2.61	66
TG-13 (50/50/0)	34.3	13.2	2.6	66
TG-14 (55/10/35)	31.4	11.7	2.7	68
TG-15 (10/80/10)	25.7	8.8	2.92	74
TG-16 (20/80/0)	30.7	11	2.78	70
TG-17 (60/20/20)	36.9	14.6	2.53	64
TG-18 (70/10/20)	38.9	15.2	2.56	65
TG-19 (0/100/0)	25.6	8.8	2.91	74
TG-20 (80/0/20)	38.1	14.6	2.62	66
TG-21 (80/10/10)	40.4	16.8	2.4	61
TG-22 (80/20/0)	37.7	15	2.51	63
TG-23 (100/0/0)	41.3	17.9	2.31	58
TG-24 (0/0/100)	1	0.3	3.84	97
TG-25 (60/10/30)	33.1	12.5	2.65	67

Table 5.8. The results of the density and other measurements of the TG samples sintered at 1650°C for 2 hours.

Blends order (SKA/SEA/CT3000SG)	Apparent Porosity, %	Water Absorption, %	Bulk Density (g/cm^3)	Theoretical Density, %
TG-1 (20/20/60)	8	2.2	3.62	91
TG-2 (10/10/80)	3.5	1	3.72	94
TG-3 (20/0/80)	9.5	2.7	3.52	89
TG-4 (20/40/40)	15.7	4.7	3.32	84
TG-5 (35/30/35)	21	6.8	3.08	78
TG-6 (0/50/50)	3.7	1	3.70	93
TG-7 (25/50/25)	21.4	6.9	3.1	78
TG-8 (5/60/35)	9.05	2.6	3.52	89
TG-9 (45/40/15)	29.4	10.6	2.78	70
TG-10 (30/60/10)	24.4	8.2	2.97	75
TG-11 (50/0/50)	20.2	6.4	3.15	80
TG-12 (50/25/25)	26.7	9.4	2.86	72
TG-13 (50/50/0)	29.9	10.9	2.74	69
TG-14 (55/10/35)	23.4	7.7	3.04	77
TG-15 (10/80/10)	19.8	6.2	3.19	81
TG-16 (20/80/0)	26.1	8.9	2.92	74
TG-17 (60/20/20)	30.7	11.3	2.72	69
TG-18 (70/10/20)	31.1	11.6	2.69	68
TG-19 (0/100/0)	20.1	6.4	3.15	80
TG-20 (80/0/20)	30.6	11.2	2.74	69
TG-21 (80/10/10)	34.5	13.45	2.57	65
TG-22 (80/20/0)	38.9	16.2	2.40	61
TG-23 (100/0/0)	39.3	16.5	2.38	60
TG-24 (0/0/100)	0.7	0.2	3.87	98
TG-25 (60/10/30)	25.8	8.8	2.92	74

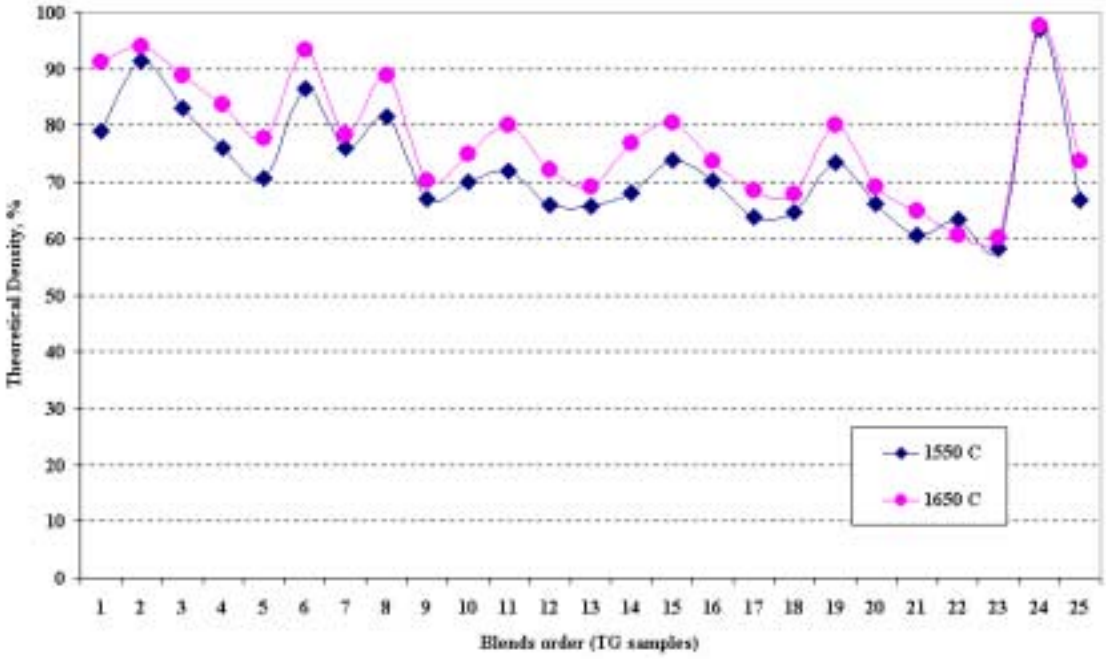

Figure 5.16. Comparison of the measured percent theoretical densities of the TG samples sintered at 1550°C and 1650°C.

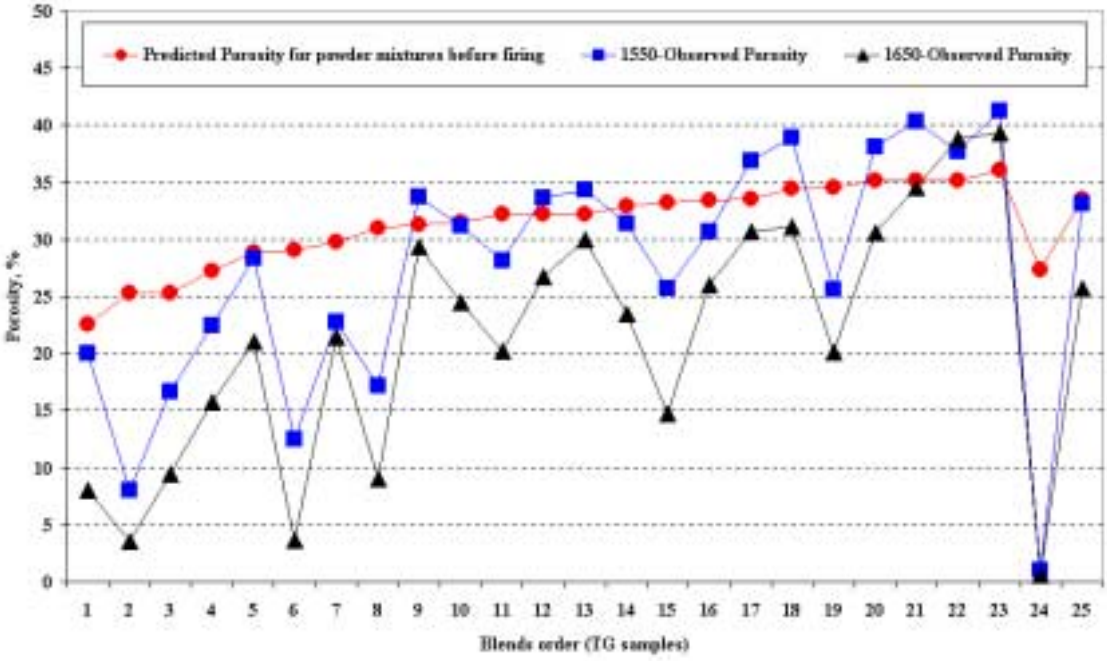

Figure 5.17. Comparison of the porosity values predicted by MXENTRY and the observed values for the TG samples sintered at 1550°C and 1650°C.

5.5.3. Binary Blends without Additives (BG)

Having understood that the coarse particles jeopardized the packing of the blends due to the presence of large agglomerates, a new set of experiments was planned for higher densities. Below, the results of the density and other measurements calculated by Archimedes' method of the compacted pellets from binary blends of ground SEA and CT3000SG powders (BG samples) sintered at 1550°C for 2 hours are given in Table 5.9. In addition to binary blends, the BG-6 (50/50) sample was further ground at 500rpm/15min hoping to further increase the density. The new powder obtained as such was labeled "extra BG". As shown in Table 5.9, this grinding only brought about a 2% increase in fired density from 87 to 89%.

Table 5.9. The results of the density and other measurements of the BG samples sintered at 1550°C.

Blends order (SEA/CT3000SG)	Apparent Porosity, %	Water Absorption, %	Bulk Density (g/cm^3)	Theoretical Density, %
BG-1 (0/100)	1.0	0.3	3.84	97
BG-2 (10/90)	0.9	0.2	3.84	97
BG-3 (20/80)	3.9	1.1	3.71	94
BG-4 (30/70)	6.8	1.9	3.63	92
BG-5 (40/60)	9.7	2.7	3.54	90
BG-6 (50/50)	12.5	3.6	3.43	87
BG-7 (60/40)	14.2	4.2	3.39	86
BG-8 (70/30)	16.5	5	3.30	84
BG-9 (80/20)	20.2	6.4	3.14	79
BG-10 (90/10)	22	7.1	3.10	78
BG-11 (100/0)	25.6	8.8	2.91	74
Extra BG-(50/50)	9.9	2.8	3.50	89

Figure 5.18 shows a comparison of the porosity values predicted by MXENTRY for unfired blends, and observed values of the BG samples sintered at 1550°C. As mentioned earlier, the maximum green packing density of BG-4 sample was predicted about 76%, however experimentally, it was realized about 7% porosity at 1550°C. As

shown in Figure 5.18, samples that contained a relatively higher proportion of CT3000SG provided higher fired densities. If the proportion of SEA is up to 50%, porosity values of the BG samples increased. Another interesting finding from this chart was that the line with circles for the predicted porosities formed a pattern similar in shape to those observed in Westman-Hugill algorithm [29]. Other notable feature of the chart in Figure 5.18 was that although the 4th circle from the left for 30% ground SEA sample on the predicted porosity line showed the least porosity before firing, the same material did not offer the lowest porosity after firing. This discrepancy results from the fact that the Alcoa alumina used was a reactive superground type with much higher sinterability.

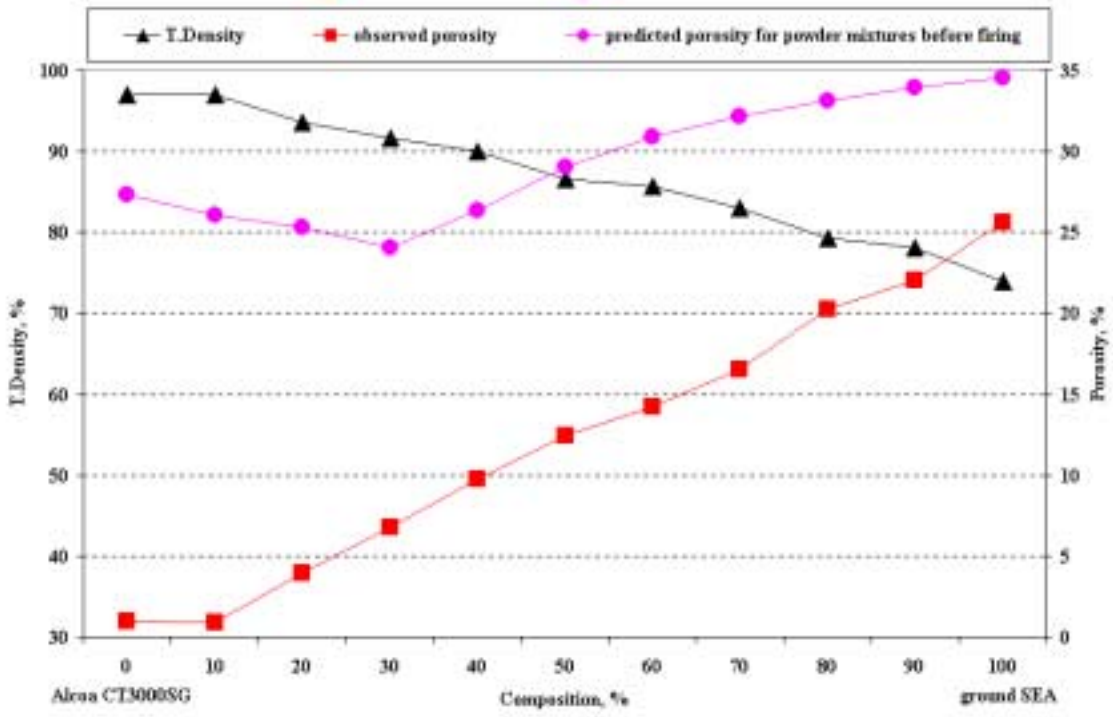

Figure 5.18. Comparison of the predicted and observed densities and porosities of the BG samples sintered at 1550°C.

5.5.4. Binary Blends with Additives (BGA)

Once the behavior of binary blends was understood, further work concentrated on the use of additives to increase sinterability, and to maximize packing. TiO_2 and MnO_2 additives were used for this purpose. Tables 5.10 and 5.11 give the results of the density and other measurements calculated by Archimedes' method of the BGA

samples with 2% TiO_2 and 3% MnO_2 additives sintered at 1550°C for 2 hours, respectively. The results showed that the additives provided higher fired densities (over 90%). Porosity and water absorption of the BGA samples is lower than 5% and 1%, respectively.

Table 5.10. The results of the density and other measurements of the BGA samples with 2% TiO_2 additive sintered at 1550°C/2h.

Blends order (SEA/CT3000SG)	Apparent Porosity, %	Water Absorption, %	Bulk Density (g/cm^3)	Theoretical Density, %
BGA-Ti-1 (0/100)	0	0	3.78	96
BGA-Ti-2 (20/80)	1.3	0.3	3.75	95
BGA-Ti-3 (40/60)	1.1	0.3	3.71	94
BGA-Ti-4 (50/50)	1.5	0.4	3.70	93
BGA-Ti-5 (60/40)	1.4	0.4	3.70	93
BGA-Ti-6 (80/20)	2.7	0.7	3.74	95
BGA-Ti-7 (100/0)	3.6	1.0	3.68	93

Table 5.11. The results of the density and other measurements of the BGA samples with 3% MnO_2 additive sintered at 1550°C/2h.

Blends order (SEA/CT3000SG)	Apparent Porosity, %	Water Absorption, %	Bulk Density (g/cm^3)	Theoretical Density, %
BGA-Mn-1 (0/100)	0.8	0.2	3.90	99
BGA-Mn-2 (20/80)	1.2	0.3	3.80	96
BGA-Mn-3 (40/60)	2	0.5	3.79	96
BGA-Mn-4 (50/50)	0.7	0.2	3.78	95
BGA-Mn-5 (60/40)	1.6	0.4	3.75	95
BGA-Mn-6 (80/20)	2.9	0.8	3.67	93
BGA-Mn-7 (100/0)	4.3	1.2	3.62	91

The theoretical densities (T.D.) of the samples with/without additives after firing at 1550°C are given in Figure 5.19. Here, it can be clearly observed that T.D. of the samples with additives (BGA) was higher than those without additives (BG). The

sintered densities of the BGA samples with MnO_2 and TiO_2 additions ranged between 91 and 99% of the theoretical densities attained. A density maximum of about 99% of TD of the BGA-Mn-1 coded sample with manganese oxide additives was obtained at 100 wt% of fine particles in the blends. The densities of the samples with manganese oxide additive (BGA-Mn) were highest up to 60 wt% coarse fraction. Titania additive was more effective at relatively higher proportion of coarse particles. The densities of the blends without additives (BG samples) were relatively lower at all fractions. To sum up, sintering aids (titania and manganese oxide) helped obtain significantly increased densification.

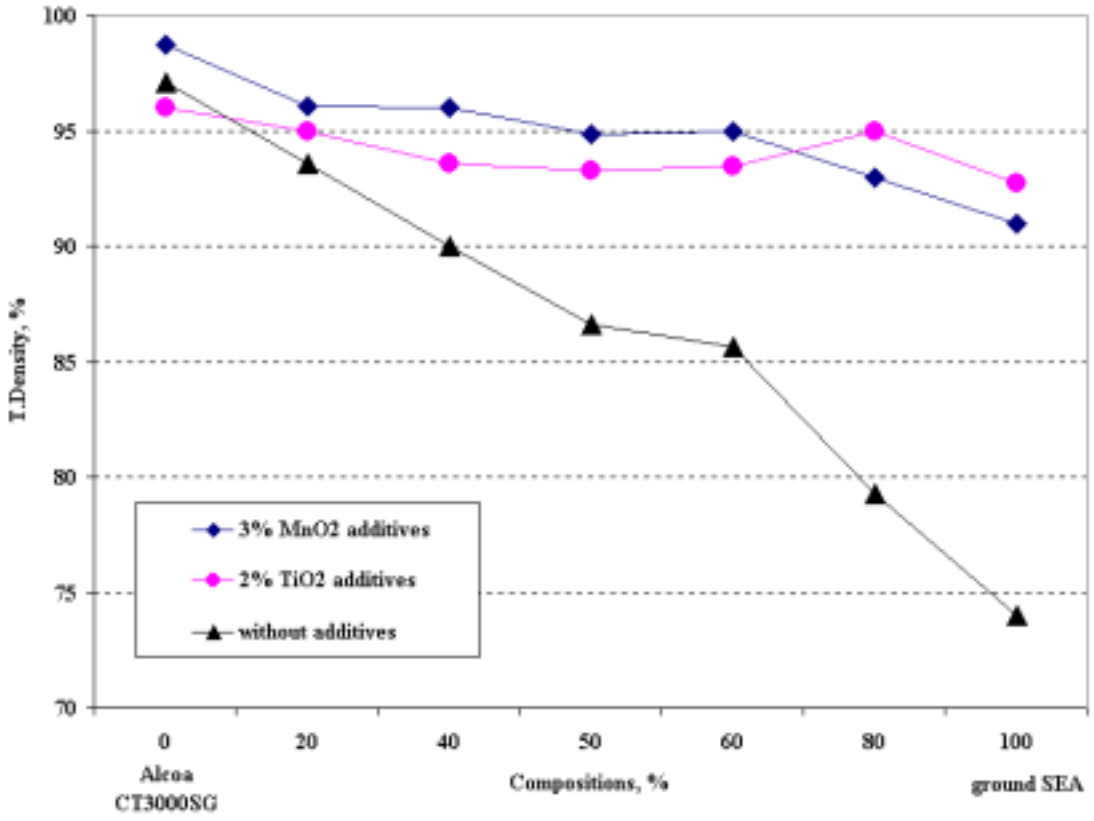

Figure 5.19. Comparison of the densities of the samples without additives (BG) and with additives (BGA-Mn and BGA-Ti) sintered at 1550°C.

5.6. Microstructural Investigations

Micrographs of some selected samples are shown in Figures 5.20, 5.21 and 5.22. As shown in Figure 5.20, normal grain growth was observed in samples (TU, TG and

BG) without additives. Also, it is clearly seen the densification rate was higher in blends that contained fine particles.

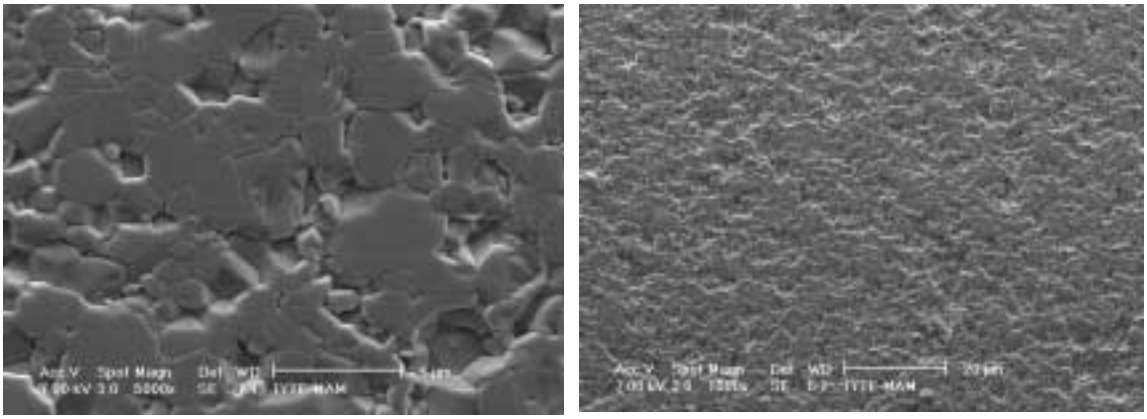

(a) Micrograph of BG-1 sample at 5000x (b) Micrograph of BG-6 sample at 1000x

Figure 5.20. SEM images at SE mode of the BG samples (without additives) sintered at 1550°C.

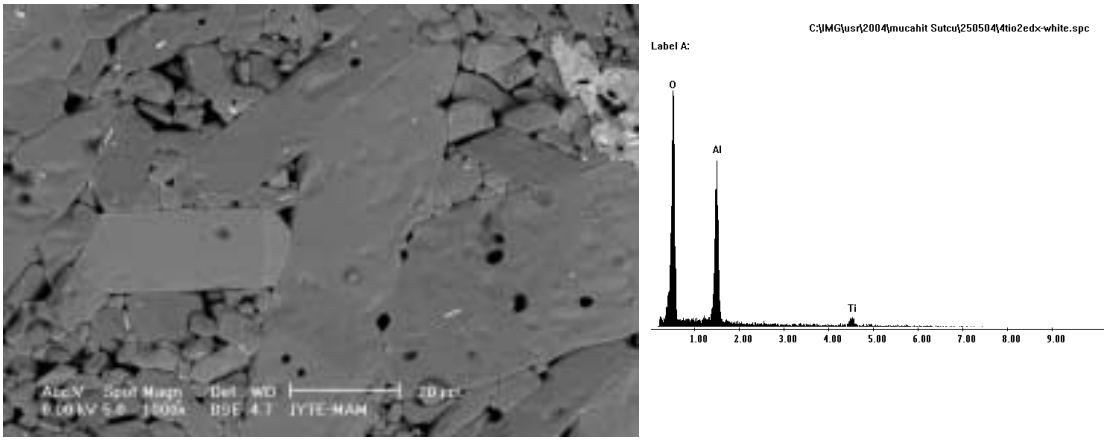

(a) (b)

Figure 5.21. (a) SEM image at BSE mode and 1000x of the BGA-Ti-6 sample sintered at 1550°C, (b) EDS-point analysis of the white particles presented in micrograph.

As shown in Figure 5.21, EDS-point analysis from light grey particles indicated that TiO_2 enters the solid solution with alumina. An exaggerated and inhomogeneous grain growth with a high amount of pores trapped and clustered within the grains was observed in some BGA-Ti samples. Excessive grain growth higher than 20 micron was observed in BGA-Ti-6 sample.

As shown in Figure 5.22, EDS-point analysis from the white particles indicated that MnO_2 entered the solid solution with alumina. An exaggerated and inhomogeneous grain growth with a low amount of porosity was observed in the samples (BGA-Mn) sintered. But excessive grain growth was lower than samples with TiO_2 additives. A eutectic composition present in the MnO_2-rich side of the binary MnO_2-$A1_2O_3$ system at 1520°C also may indicate the formation of a small amount of liquid phase at 1550°C [25].

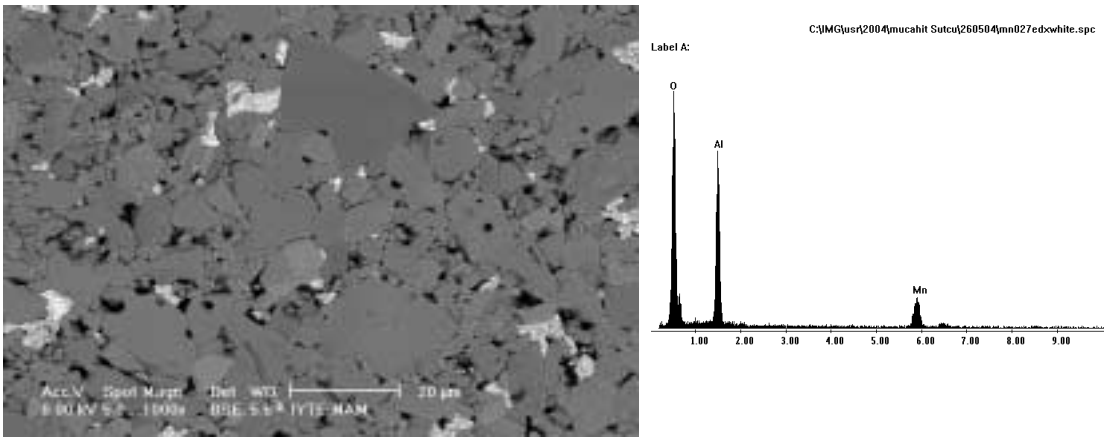

(a) (b)

Figure 5.22. (a) SEM image at BSE mode and 1000x of the BGA-Mn-6 sample sintered 1550°C, (b) EDS-point analysis of the white parts presented in micrograph.

5.7. Mechanical Measurements

Mechanical properties of the binary blends (BG and BGA samples) were investigated. The other lower density samples were, however, not tested. Figure 5.23 shows the comparison of Vickers hardness-testing results of the BG samples (without additives) and BGA samples (with additives) sintered at 1550°C that applied 500 grams (4.9N) of load.

As shown in Figure 5.23, the BG samples (binary blends without additives) that contained relatively higher proportions of fine particles provided higher hardness values. Generally, the use of coarse particles in blends brought about lower mechanical properties. Usually for many applications a micro-hardness Vickers (HV) value of 1250 $kg.mm^{-2}$ is sufficient. The results for BGA samples (binary blends with additives) were, however, in a much narrower range of 1100 and 1700 $kg.mm^{-2}$.

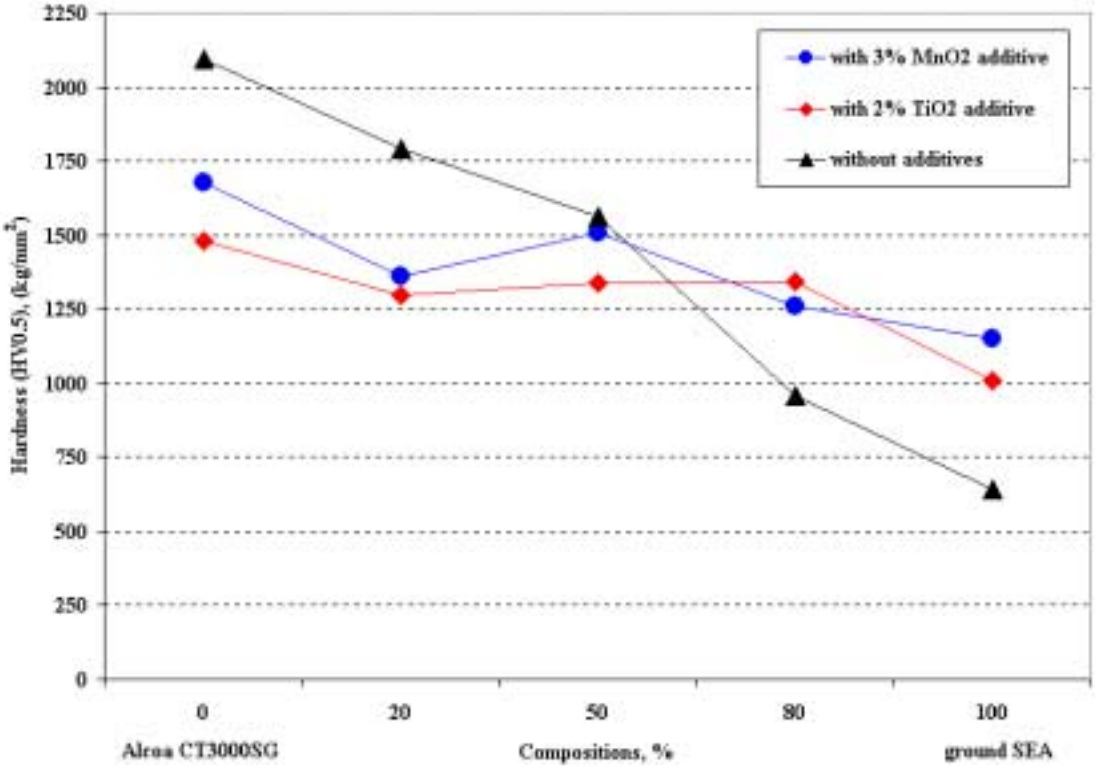

Figure 5.23. Comparison of the Vickers hardness values of the samples without additives (BG) and with additives (BGA-Mn and BGA-Ti) sintered at 1550°C.

In Figure 5.24 a photograph of the pressed and fired tiles contained 100% CT3000SG powder (BG-1 or TG-24 blends) is shown. Some selected measured properties of produced tiles are listed in Table 5.17. Similar densities could be produced via slip casting and dry pressing. The Vickers hardness (HV) values for dry pressed tiles were a little higher than the slip cast tile.

Table 5.17. Measured properties of the tiles.

	Slip cast tile	Dry pressed tile
Theoretical Density, %	95	96
Hardness (HV10), $kg.mm^{-2}$	1690	1765

Figure 5.24. Photograph of dry pressed alumina tile sintered at 1550°C (70x70x20 mm).

Chapter 6

CONCLUSIONS

In this study, densification and mechanical properties of the ceramic pellets and tiles produced from mixtures of alumina powders with different particle size distributions (PSD) were investigated. The powders used were domestic (SKA-coarse and SEA-medium particle size) powders and a reactive fine Alcoa CT3000SG powder.

Before the domestic powders were used, pre-treatments were applied to improve the raw material quality such as washing and re-calcination. As a result of washing treatments of the powders, hot washing treatment was found to be effective in lowering the sodium oxide (Na_2O) content of SKA and SEA powders down to 0.11% and 0.25% from about 0.4% and 0.8%, respectively. Also, these powders were completely transformed into the stable alpha phase upon calcination at 1250°C.

Particle size distributions (PSD) of domestic powders were reduced to suitable size intervals (about 2:1 ratio) via milling that also improved packing.

MX computer software (MXENTRY ® and MIX10 ®) was used to predict the green density of the powder compact and to calculate the compositions of the blends (TU, TG and BG) that would pack most densely in the green state.

Density and porosity measurements of the sintered pellets and tiles were done by Archimedes' method. In the TU and TG samples, when the sintering temperature was increased, fired density of the pellets also increased. Consequently, the porosity and water absorption of the pellets decreased. All results showed that the TG-24 (0/0/100) sample contained 100% fine-reactive alumina powder achieved almost full density (98%) at both temperatures. Also, TG-1 (20/20/60), TG-2 (10/10/80), TG-3 (20/0/80), TG-6 (0/50/50) and TG-8 (5/60/35) samples achieved low porosity and water absorption levels for both temperatures. These samples, especially at 1650°C, may be preferred for mechanical uses. For the other samples, porosity values of the blends that contained a relatively higher proportion of coarse particles were higher than predicted. This result was not expected and probably resulted from the effect of inefficient mixing for predicted packing. Particles were probably unable to rearrange during sintering due to coarse agglomerate sizes.

BG-blends with a higher proportion of CT3000SG provided higher fired densities. If the proportion of SEA was close to 50%, porosity values of the blends significantly increased.

2% TiO_2 and 3% MnO_2 additions were used to increase sinterability and to maximize packing. Higher fired densities between 91 and 99% were achieved. Theoretical densities of BGA-blends were higher than those without additives. The densities of the blends with manganese oxide additive (BGA-Mn) were highest up to 60 wt% coarse fraction. Titania additive was more effective at relatively higher proportion of coarse particles. The densities of the BG-blends were relatively lower at all fractions. To sum up, the sintering aids (TiO_2 and MnO_2) helped obtain significantly increased densification.

Microstructural investigations indicated that normal grain growth occurred in TU, TG and BG samples. Also, the densification rate was higher in blends that contained fine particles. In the BGA samples, EDS-point analysis indicated that TiO_2 and MnO_2 additives entered in solid solution with alumina. An exaggerated and inhomogeneous grain growth with a high amount of pores trapped and clustered within the grains was observed in some BGA-Ti samples. Besides, in the BGA-Mn samples, excessive grain growth was lower than BGA-Ti samples.

Vickers hardness test was performed for mechanical property measurements. The BG samples that contained relatively higher proportions of fine particles provided higher hardness values in a range of 1500 and 2100 $kg.mm^{-2}$. Generally, the use of coarse particles in blends brought about lower mechanical properties. The BGA samples were, however, in a much narrower range of 1100 and 1700 $kg.mm^{-2}$.

Further work may include mechanical characterization for compressive, flexural, impact and fracture toughness properties of tiles. For the use of domestic powders in technical ceramic applications they should be well ground with grinding aids. Studies on the domestic electrofilter-residue alumina powders should be continued. Also different sintering aids may be tried to prevent excessive grain growth in the tiles.

REFERENCES

[1] McLeod, C.T., Kasiner, J.W., Carbone, T.J. and Starr, J.P., "Aluminas for Tomorrow's Ceramics", *Ceramic Engineering and Science Proceedings*, Vol.6, No.9-12, 1985.

[2] Gitzen, W.H., "Alumina as a Ceramic Material", Special Publication No: 4, The American Ceramic Society, Ohio, 1970.

[3] Powell-Doğan, C.A., Heuer, A.H., "Microstructure of 96% Alumina Ceramics: I, II, III", *Journal of American Ceramic Society*, 73 (12), 3670-91, 1990

[4] Matchen, B., "Applications of Ceramics in Armor Products", *Key Engineering Materials*, Vols.122-124, Pp. 333-42, Advanced Ceramic Materials, Edited By H. Mostaghasi, Trans Tech Publications, Switzerland, 1996.

[5] Medvedovski, E., "Alumina Ceramics for Ballistic Protection, Part 1-2", *American Ceramic Society Bulletin*, Vol.81, No.3-4, 2002.

[6] Erkalfa, H., Mısırlı, Z., Baykara, T., "Effect of Additives on the Densification and Microstructural Development of Low-grade Alumina Powders", *Journal of Materials Processing Technology*, Vol. 62, 1996, 108-115.

[7] Lange, F.F., Velamakanni, B.V., "Method for Preparation of Dense Ceramic Products", United States Patent 5.188.780, 1993.

[8] Niesz, D.E., Brockway, M.C., "Densification in High-Modulus Ceramics, in DCIC Report", Ceramic Armor Technology, Defence Ceramic Information Center, 69-1, 1969.

[9] Dinger, D.R., Funk, J.E., "Predictive Process Control of Crowded Suspensions", JEFCO Ceramic Consultants, Seneca, 1993.

[10] Andreassen, A.H.M., Andersen, J., "Ueber die Beziehung zwischen Kornabstufung und Zwischenraum in Producten aus Losen Koernern (Mit Einigen Experimenten)", *Kolloid-Z*, 50, 217-228, 1930.

[11] Plunkert, P.A., "Bauxite and Alumina", U.S. Geological Survey Minerals Yearbook, 2002.

[12] DPT Sekizinci Beş Yıllık Kalkınma Planı, "Madencilik Özel İhtisas Komisyonu Raporu, Metal Madenler Alt Komisyonu-Boksit Çalışma Grubu Raporu", DPT, Ankara, 2001.

[13] UNCTAD Secretariat "Recent and Planned Changes in Production Capacity for Bauxite, Alumina and Aluminum", United Nations Conference on Trade and Development (UNCTAD), 2000.

[14] www.altech.pechiney.com.

[15] Şahin, S., "Boksitlerden Bayer Prosesi ile Alumina Üretiminde Yer Alan Su Giderme İşleminin Teknolojik Esasları", *Journal of Qafqaz University*, Number 6, Fall 2000.

[16] Kırk-Othmer Encyclopedia of Chemical Technology, "Aluminum Compounds (Aluminum Oxide)", Vol.2, Pages 233-240.

[17] Reed, J.S., "Principles of Ceramics Processing", Second Edition, A Wiley-Interscience Publication, John Wiley &Sons, New York, 1995.

[18] Bengisu, M., "Engineering Ceramics", Springer-Verlag, New York, 2001.

[19] "CRC Handbook of Materials Science", Volume II: Metals, Composites and Refractory Materials, Editor: C.T. Lynch, Pages 357-362, 1990.

[20] Samer, Ş., Toy, Ç., Tekin, A., "AlF_3 Katkısının Seydişehir Alumina Toz Özelliklerine Etkisi", 8. Uluslararası Metalurji ve Malzeme Kongresi, Bildiriler Kitabı, Sayfa 547-554, 6-9 Haziran 1995, İstanbul, Türkiye.

[21] Mistler, R.E., Shanefield, D.J., "Washing Ceramic Powders to Remove Sodium Salts", *American Ceramic Society Bulletin*, Vol. 57, No. 7, P. 689, 1978.

[22] Tambaş, T., "Seydişehir Aluminasından Kalıplamayla Seramik Malzemelerin Üretilmesi", Yüksek Lisans Tezi, İ.T.Ü. Fen Bilimleri Enstitüsü, 1998.

[23] Kingery, W.D., Bowen, H.K., Uhlmann, D.R., "Introduction to Ceramics", Second Edition, A Wiley-Interscience Publication, John Wiley &Sons, New York, 1976.

[24] Rahaman, M.N., "Ceramic Processing and Sintering", Marcel Dekker Inc., New York, 1995.

[25] Erkalfa, H., Mısırlı, Z., Baykara, T., "The Effect of TiO_2 and MnO_2 on Densification and Microstructural Development of Alumina", *Ceramic International*, 24, 1998, 81-90.

[26] Sathiyakumar, M., Gnanam, F.D., "Influence of MnO and TiO_2 Additives on Density, Microstructure and Mechanical Properties of Al_2O_3", *Ceramic International*, 28, 2002, 195-200.

[27] Furnas, C.C., "Reletions Between Specific Volume, Voids and Size Composition in Systems of Broken Solids of Mixed Sizes", U.S. Bureau of Mines Report of Investigations, No. 2894, 1928.

[28] McGeary, R.K., "Mechanical Packing of Spherical Particles", *Journal of American Ceramic Society*, 44, 413-422, 1961.

[29] Westman, A.E.R., Hugill, H.R., "The Packing of Particles", *Journal of American Ceramic Society*, 13, [10], 767-779, 1930.

[30] Fuller, W.B., Thompson, S.E., "The Laws of Proportioning Concrete", *Proceedings American Society Civil Engineering*, 33, 261, 1907.

[31] "Ürün Kataloğu", E11 SEY KAT DC 02 01 (R1), Eti Aluminyum A.Ş. Genel Müdürlüğü.

[32] Alcoa Industrial Chemicals Europe, Calcined and Reactive Aluminas for the Ceramic Industry Product Data.

[33] Underwood, E.E., Colcord, A.R., Waugh, R.C., "Quantitative Relationships for Random Microstructures", Chapter 1, Ceramic Microstructures, Proceedings of the 3rd International Materials Symposium, June 13-16, 1966.

[34] DeHoff, R.T., "Problem Solving Using Quantitative Stereology", "Applied Metallography", p. 89-99, G.F. Vander Voort, Editor Van Nostrand Reinhold, NewYork, 1986.

[35] Engqvist, H., Uhrenius, B., "Determination of the Average Grain Size of Cemented Carbides", *International Journal of Refractory Metals & Hard Materials*, 21, 2003, 31–35.

[36] Allen, T., "Particle Size Measurements", John Wiley&Sons, New York, 1974.

[37] Standard Test Methods for Apparent Porosity, Water Absorption, Apparent Specific Gravity, and Bulk Density of Burned Refractory Brick and Shapes by Boiling Water, ASTM Designation: C20-87, "Annual Book of ASTM Standards", Vol.15.01, 1987.

APPENDICES

APPENDIX A

Table A.1. MX file for unground SKA powders.

Size (μm)	CPFT	% in Class	Surface Area (m^2/cc)	Cumulative SA (m^2/cc)	Calculated Porosity, %	# in Class	Cumulative # PCI
26.08	11.83						
31.03	16.05	4.22	0.01335	0.13	28.26	.350D+07	.130D+08
36.91	21.78	5.72	0.01522	0.12	29.06	.282D+07	.955D+07
43.9	29.54	7.76	0.01736	0.1	30.15	.227D+07	.673D+07
52.22	39.78	10.2	0.01926	0.09	31.58	.178D+07	.445D+07
62.12	49.4	9.61	0.01519	0.07	32.92	.994D+06	.267D+07
73.89	61.46	12.1	0.01603	0.05	34.61	.741D+06	.168D+07
87.9	77.88	16.4	0.01833	0.04	35.29	.599D+06	.935D+06
104.6	88.88	11	0.01033	0.02	34.77	.238D+06	.336D+06
124.4	93.78	4.9	0.00387	0.01	35.22	.632D+05	.978D+05
147.9	96.82	3.04	0.00202	0	35.35	.233D+05	.347D+05
176	98.42	1.6	0.00089	0	37.35	.727D+04	.114D+05
209.3	99.9	1.47	0.00069	0	37.51	.397D+04	.414D+04
249	100	0.105	0.00004	0	40	.168D+03	.168D+03

Table A.2. MX file for unground SEA powders.

Size (μm)	CPFT	% in Class	Surface Area (m^2/cc)	Cumulative SA (m^2/cc)	Calculated Porosity, %	# in Class	Cumulative # PCI
2.73	10.45						
3.25	17.06	6.61	0.19959	1.63	30.17	.477D+10	.186D+11
3.87	27.84	10.80	0.2739	1.43	31.45	.463D+10	.138D+11
4.60	45.45	17.60	0.37589	1.15	33.11	.449D+10	.918D+10
5.47	60.28	14.80	0.26614	0.78	34.98	.225D+10	.469D+10
6.51	78.65	18.40	0.27711	0.51	34.81	.165D+10	.244D+10
7.74	88.15	9.51	0.12056	0.23	35.59	.508D+09	.791D+09
9.21	94.49	6.34	0.06761	0.11	35.87	.201D+09	.283D+09
10.95	97.67	3.17	0.02842	0.04	36.41	.598D+08	.818D+08
13.03	99.23	1.57	0.01182	0.02	36.58	.176D+08	.219D+08
15.50	99.78	0.54	0.00344	0	35.87	.362D+07	.435D+07
18.43	99.91	0.13	0.00068	0	37.51	.506D+06	.727D+06
21.93	100.00	0.09	0.00042	0	40	.221D+06	.221D+06

Table A.3. MX file for Alcoa CT3000SG powders.

Size (μm)	CPFT	% in Class	Surface Area (m^2/cc)	Cumulative SA (m^2/cc)	Calculated Porosity, %	# in Class	Cumulative # PCI
0.2022	9.814						
0.2405	15.9	6.09	2.48349	20.94	29.32	.108D+14	.420D+14
0.2861	25.76	9.86	3.38248	18.46	30.58	.104D+14	.312D+14
0.3404	41.74	16	4.60688	15.07	31.43	.100D+14	.208D+14
0.4049	55.22	13.5	3.27019	10.47	33.42	.504D+13	.107D+14
0.4816	70.29	15.1	3.07145	7.2	33.51	.334D+13	.571D+13
0.5729	80.47	10.2	1.74373	4.13	34.62	.134D+13	.237D+13
0.6815	88.81	8.34	1.20143	2.38	35.18	.653D+12	.102D+13
0.8106	94.23	5.42	0.65647	1.18	35.44	.252D+12	.372D+12
0.9643	97.2	2.97	0.30239	0.52	35.96	.821D+11	.120D+12
1.147	98.86	1.65	0.14135	0.22	37.2	.271D+11	.377D+11
1.364	99.87	1.01	0.0726	0.08	37.51	.984D+10	.106D+11
1.623	100	0.134	0.00812	0.01	40	.778D+09	.778D+09

APPENDIX B

Table B.1. MX file for ground SKA powders.

Size (μm)	CPFT	% in Class	Surface Area (m^2/cc)	Cumulative SA (m^2/cc)	Calculated Porosity, %	# in Class	Cumulative # PCI
26.08	61.44						
31.03	67.97	6.53	0.02067	0.08	31.19	.542D+07	.133D+08
36.91	75.2	7.23	0.01923	0.06	33.18	.356D+07	.789D+07
43.9	83.2	8	0.01788	0.04	35.28	.234D+07	.433D+07
52.22	91.53	8.33	0.01566	0.03	33.49	.145D+07	.199D+07
62.12	94.42	2.89	0.00456	0.01	35.32	.299D+06	.539D+06
73.89	97.21	2.8	0.00371	0.01	34.47	.172D+06	.240D+06
87.9	98.37	1.15	0.00129	0	35.53	.421D+05	.688D+05
104.6	99.23	0.861	0.00081	0	36.04	.187D+05	.268D+05
124.4	99.69	0.467	0.00037	0	36.65	.601D+04	.810D+04
147.9	99.92	0.222	0.00015	0	37.51	.170D+04	.208D+04
176	100	0.0844	0.00005	0	40	.384D+03	.384D+03

Table B.2. MX file for ground SEA powders.

Size (μm)	CPFT	% in Class	Surface Area (m^2/cc)	Cumulative SA (m^2/cc)	Calculated Porosity, %	# in Class	Cumulative # PCI
2.732	41.93						
3.25	51.08	9.15	0.27639	1.22	31.93	.661D+10	.173D+11
3.866	62.22	11.1	0.28306	0.94	33.77	.478D+10	.107D+11
4.598	75.8	13.6	0.28982	0.66	34.1	.346D+10	.594D+10
5.47	85.07	9.27	0.16642	0.37	36.35	.140D+10	.248D+10
6.506	94.94	9.87	0.1489	0.2	34.98	.888D+09	.108D+10
7.74	97.28	2.34	0.02966	0.06	35.42	.125D+09	.189D+09
9.206	98.68	1.4	0.01488	0.03	35.84	.443D+08	.640D+08
10.95	99.43	0.755	0.00677	0.01	36.28	.143D+08	.197D+08
13.03	99.8	0.368	0.00277	0	37.34	.412D+07	.542D+07
15.5	99.99	0.186	0.00118	0	37.51	.124D+07	.129D+07
18.43	100	0.014	0.00007	0	40	.553D+05	.553D+05